Chemical Synthesis Using Metal Atoms. Matrix Infrared, Raman, Ultraviolet–Visible, and Electron Spin Resonance Studies of the Binary Carbonyls of Cobalt, $Co(CO)_n$ (where n = 1–4), and the Distortion Problem in $Co(CO)_4$

L. A. Hanlan, H. Huber, E. P. Kündig, B. R. McGarvey, and G. A. Ozin*

Contribution from Erindale College and the Lash Miller Chemistry Laboratories, University of Toronto, Toronto, Ontario, Canada. *Received May 1, 1975*

Abstract: The cocondensation reactions of Co atoms with CO at 6–15 K are investigated for the first time using matrix infrared, Raman, uv–visible, and ESR spectroscopy. Using extremely low Co concentrations (Co:M $\simeq$ 1:10^4 to 1:10^5) which are shown to favor the formation of mononuclear complexes, variable concentration $^{12}C^{16}O$–M experiments (where M = Ne, Ar, Kr, or Xe), $^{12}C^{16}O$–$^{13}C^{16}O$ and $^{12}C^{16}O$–$^{12}C^{18}O$–M mixed isotopic substitution, in conjunction with matrix warm-up experiments, the reaction products are shown to be $Co(CO)_n$ (where n = 1–4). The vibrational spectroscopic data and isotope frequency calculations for $Co(^{12}C^{16}O)_n(^{13}C^{16}O)_{4-n}$ (where n = 0–4) in carbon monoxide matrices favor a C_{3v} trigonally distorted tetrahedral structure for $Co(CO)_4$. The corresponding ESR spectrum supports the contention that the molecule has axial symmetry and S = ½. The spin-Hamiltonian parameters are $g_\parallel = 2.007 \pm 0.010$, $g_\perp = 2.128 \pm 0.010$, $A_\parallel(^{59}Co) = (58 \pm 1) \times 10^{-4}$ cm^{-1}, and $A_\perp(^{59}Co) = (55 \pm 1) \times 10^{-4}$ cm^{-1} and are found to be consistent with a C_{3v} trigonal distortion. Striking confirmation of the C_{3v} distortion is obtained from the ^{13}C hyperfine splitting of $Co(^{13}C^{16}O)_4$ in 93% $^{13}C^{16}O$. The corresponding uv–visible spectrum displays ligand field and charge transfer bands in the region 200–350 nm. The appropriate relationship between the electronic and magnetic parameters of C_{3v} $Co(CO)_4$ provides an order of magnitude estimate for the ligand field parameter Δ and predicts the $^2A_1 \rightarrow {}^2E$ d–d transition in the range 300–350 nm. The ESR data for $Co(CO)_4$ in Ar matrices provide evidence for two forms of the molecule, $Co(CO)_4$ (I) and $Co(CO)_4$ (II). Both molecules appear to have axial symmetry and S = ½ but with different spin-Hamiltonian parameters and different ^{13}C hyperfine splittings. $Co(CO)_4$ (I) is favored on deposition at 6–8 K while $Co(CO)_4$ (II) predominates upon annealing the matrix to 30–35 K. An analysis of the data is not totally unambiguous, although the ESR parameters for $Co(CO)_4$ in Ar matrices can be interpreted in terms of two isomeric forms of $Co(CO)_4$, one having a C_{3v} distortion (I) and the other a D_{2d} distortion (II). The observed higher stability of molecule II in Ar supports the conclusions drawn from minimum internal energy molecular orbital calculations which favor the D_{2d} configuration. Infrared isotope frequency calculations were performed for the C_{3v} (I) and D_{2d} (II) isomeric forms of $Co(^{12}C^{16}O)_n(^{13}C^{16}O)_{4-n}$ (where n = 0–4) in Ar matrices. In contrast to the data for $Co(CO)_4$ in CO matrices, the compared frequencies for C_{3v} and D_{2d} $Co(CO)_4$ in Ar matrices fit the experimental data equally well and reinforce the conclusions drawn from the corresponding ESR data. The vibrational data for $Co(CO)_3$ in inert gas matrices suggest that the molecule has a regular triangular planar D_{3h} structure. However, the absence of observable ^{13}C hyperfine splitting in the corresponding $Co(^{13}C^{16}O)_3$ ESR spectrum implies that $Co(CO)_3$ is most probably distorted away from planar toward a C_{3v} trigonal pyramidal structure. The vibrational data for $Co(CO)_2$ and Co(CO) appear to favor linear $D_{\infty h}$ and $C_{\infty v}$ structures, respectively. The Co–CO matrix reaction is also investigated at high Co concentrations (1/100) and by comparison with matrix-isolated $Co_2(CO)_8$ is shown to yield a mixture of the cobalt–cobalt bonded and CO-bridge bonded isomers of $Co_2(CO)_8$. The results of these experiments serve to demonstrate that matrix surface diffusion reactions far exceed in importance the statistical generation of binuclears. Best fit Cotton–Kraihanzel k_{CO} force constants are determined for $Co(CO)_n$ (where n = 1–4) and are discussed in the light of the analogous data for the d^{10} $Ni(CO)_n$ complexes. The matrix-induced frequency shifts observed for $Co(CO)_n$ (where n = 1–4) in Ne, Ar, Kr, Xe, and CO matrices are rationalized in terms of Buckingham's theory of nonspecific solute–solvent interactions. Finally, molecular distortions arising from electronic effects in binary transition metal carbonyl fragments $M(CO)_n$ (where n = 4 and 3) are briefly discussed in the light of recent experimental results and molecular orbital calculations.

Since the original 1910 discovery of dicobalt octacarbonyl by Mond, Hirtz, and Cowap,[1] considerable attention has been focused on cobalt carbonyls and their derivatives, particularly in terms of their catalytic activity and selectivity in a wide variety of industrially important carbonylation and hydroformylation reactions.[2] Coordinatively unsaturated cobalt carbonyl derivatives have often been postulated as catalytic intermediates in these processes[3] but generally speaking these reactive species have been poorly characterized. In principle, an insight into the molecular and electronic properties and reactivities of these species can be obtained from studies of the analogous coordinatively unsaturated binary carbonyls of cobalt $Co(CO)_n$. However, up to the time of writing, surprisingly little information is available for such compounds. The data that have been reported so far refer exclusively to $Co(CO)_4$. Often the results have led to ambiguous conclusions and conflicting opinions as to the exact nature of the molecule.

In brief, the tetracarbonyl cobalt free radical $Co(CO)_4$ was first detected by Keller and Wawersik[4] as a paramagnetic species obtained by sublimation of $Co_2(CO)_8$ onto a 77 K cold finger held in the microwave cavity of an ESR spectrometer. This was later confirmed by Symons et al.[5] Bidinosti and McIntyre[6] were able to detect $Co(CO)_4$ mass spectrometrically from the Knudsen cell pyrolysis of $Co_2(CO)_8$. More recently, Rest et al.[7] synthesized $Co(CO)_4$ by photolyzing $Co(CO)_3(NO)$ in either CO or CO–Ar matrices at 20 K. Their matrix infrared isotopic substitution experiments, which were conducted in *pure* $^{12}C^{16}O$–$^{13}C^{16}O$ mixtures, led them to believe that the $Co(CO)_4$ so produced must have a stereochemistry distorted away from regular tetrahedral. The ESR data for $Co(CO)_4$[4,5] in a $Co_2(CO)_8$ matrix are also consistent with a distortion away from regular tetrahedral symmetry and were shown[5] to be consistent with C_{3v} symmetry. Finally, infrared frequency and absorbance calculations for the mixed isotopic molecules Co-

$(^{12}C^{16}O)_n(^{13}C^{16}O)_{4-n}$ (where n = 0-4) have been performed for C_{3v} and D_{2d} symmetries and appear to favor the C_{3v} distortion for the complex in a solid CO matrix.[7]

However, a criticism of this approach to the distortion problem in $Co(CO)_4$ is that the conclusion is based on data obtained in CO and $Co_2(CO)_8$ lattices having low substitutional site symmetries and as such could be responsible for the trigonal distortion proposed for the entrapped molecule.

At about the same time as Rest et al.[7] observed $Co(CO)_4$ we[8] had independently reported preliminary matrix infrared and Raman observations for $Co(CO)_4$ synthesized from Co atoms and CO and had concluded at the time that our vibrational data were more consistent with the D_{2d} distortion for $Co(CO)_4$. Since then, we have obtained detailed infrared data for $Co(CO)_4$ in a variety of different matrices as well as the corresponding mixed isotopic substitution data, matrix uv-visible, and ESR $^{12}C^{16}O$ and $^{13}C^{16}O$ isotopic data. The results have proven to be surprisingly revealing and appear to clarify most aspects of the $Co(CO)_4$ problem. Moreover, we have extended our matrix infrared experiments and have been able to synthesize and characterize the coordinatively unsaturated intermediate carbonyls Co(CO), $Co(CO)_2$, and $Co(CO)_3$. These serve to complete the spectroscopic data for the binary cobalt carbonyls and enable one to examine the trends in their vibrational spectra, force constants, molecular and electronic structures, and stabilities, as well as making possible interesting comparisons with their d^{10} neighbors $Ni(CO)_n$ (where n = 1-4). In this paper we report these data.

Experimental Section

Monatomic Co was generated by directly heating a thin (0.015 in.) ribbon filament of Co with ac. The cobalt metal (99.99%) was supplied by McKay, Inc., New York. Research grade $^{12}C^{16}O$ (99.99%) was supplied by Matheson of Canada and $^{12}C^{16}O$-$^{13}C^{16}O$, $^{12}C^{16}O$-$^{12}C^{18}O$ isotopic mixtures by Stohler, Montreal. The furnace used for the evaporation of the metals has been described previously.[9] The rate of metal atom deposition was continuously monitored using a quartz crystal microbalance.[10] To obtain quantitative data for Co-CO and Co-CO-M (M = Ne, Ar, Kr, or Xe) cocondensations it was necessary to calibrate carefully the rate of deposition of both metal and gas onto the sample window as described previously.[11] In the infrared experiments, matrices were deposited on a CsI plate cooled to 10-12 K by means of an Air Products Displex closed-cycle helium refrigerator or to 6 K by a liquid helium transfer system. Spectra were recorded on a Perkin-Elmer 180 spectrophotometer. In the Raman experiments, successful only for $Co(CO)_4$ in CO, the matrices were deposited onto a highly polished aluminum tip cooled to 6 K. Raman spectra were recorded on a Spex Model 1401 double monochromator using Carson argon ion 4880 and 5145 Å laser excitation. Uv-visible spectra were recorded on a standard Unicam S.P. 8000 instrument in the range 190-700 nm, the sample being deposited onto a NaCl optical plate cooled to 6 K. In the ESR experiments, the sample was deposited onto a sapphire rod (dimensions 1.75 × 0.12 × 0.04 in.) cooled to 6 K. Using a specially designed telescopic vacuum shroud[12] the sample could be lowered into an extension quartz tailpiece, held in the microwave cavity of a standard Varian E4 spectrometer. ESR spectra were recorded in the range 0-6000 G with microwave powers varied between 0.1 and 10 mW for optimum resolution conditions.

Typical conditions which favored the matrix reactions of Co atoms and the formation of mononuclear complexes $Co(CO)_n$ were Co:CO $\leq$ 1:10^4. Binuclear complex formation becomes appreciable in the range 1:10^4 $\leq$ Co:CO $\leq$ 1:10^2.

Results and Discussion

Unlike previous investigations of the Ni-CO, Pd-CO, and Pt-CO cocondensation reactions[13] in which product characterization was found to be a relatively straightforward procedure, the Co-CO reaction proved to be particularly awkward because of a pronounced tendency towards dimerization, especially in Ne-CO, Ar-CO, and CO matrices. Facile formation of binuclear reaction products $Co_2(CO)_n$ was apparent even at concentration levels where the statistical generation of binuclear species was expected to be negligibly small. This phenomenon has been previously encountered[11,14] (and in fact used to advantage in the synthesis of novel binuclear carbonyl complexes such as $Rh_2(CO)_8$, $Ir_2(CO)_8$,[11] and $Cu_2(CO)_6$[14c]) and has been analyzed in terms of an alternative pathway to binuclear product formation involving surface diffusion during matrix deposition. The surface diffusion pathway could be arranged to be negligibly small by experimenting at extremely low metal/matrix ratios and (or) with highly polarizable, rigid matrices such as Kr and Xe.[14] Only under these conditions was it possible to obtain Co atom reactions and mononuclear reaction products.

In contrast to the d^{10} carbonyls $Ni(CO)_n$ (where n = 1-4) whose molecular structures were found to be those with the highest symmetry,[13b] one would not necessarily expect the d^9 cobalt analogues to behave similarly, as Jahn-Teller instability, for example, may cause distortions away from the most regular structures. One must therefore distinguish genuine molecular distortions from, for example, lattice site effects and/or multiple trapping site effects. The results for each of the $Co(CO)_n$ species (where n = 1-4) will now be discussed in turn.

Tetracarbonyl Cobalt, $Co(CO)_4$; Matrix Infrared Experiments in Pure CO. When Co atoms were cocondensed with pure $^{12}C^{16}O$ at low cobalt concentrations (Co:CO $\simeq$ 1:10^5) at 10-15 K two main absorptions were observed in the CO stretching region at 2028.8 and 2010.7 cm^{-1} with a weak shoulder at 2001.8 cm^{-1} (Figure 1A). The 2028.8/2010.7 cm^{-1} absorptions appeared with the same relative intensities in a number of different runs and maintained the same intensity ratio during warm-up experiments. On the other hand, the weak shoulder at 2001.8 cm^{-1} grows in during matrix warm-up experiments at 35-45 K together with absorptions assignable to $Co_2(CO)_8$ (see later), whereas the 2028.8/2010.7 cm^{-1} absorptions gradually decrease in intensity. Moreover, the relative intensities of the 2028.8/2010.7 cm^{-1} doublet compared to the 2001.8 cm^{-1} absorption are dependent on the Co concentration, the latter being favored at high Co/CO ratios. These data suggest that the 2001.8-cm^{-1} absorption is most likely associated with an aggregate species $Co_x(CO)_y$. (The 2001.8-cm^{-1} line does not appear when the experiment is performed at 6 K and Co:CO < 1:10^5.) It is noteworthy that the complex absorbing at 2028.8/2010.7 cm^{-1} has an infrared spectrum essentially identical with that obtained by Rest et al.[7] for $Co(CO)_4$ produced by the photolysis of $Co(CO)_3(NO)$ in CO matrices. This agreement is especially gratifying as the two approaches to the generation of $Co(CO)_4$ are quite different.

Further evidence that supports the tetracarbonyl formulation for the product of the Co-CO reaction stems from five other sources, listed below, each of which will be elaborated on in later sections. (a) *Three other* binary, mononuclear carbonyls $Co(CO)_n$ (where n = 1-3) can be synthesized in dilute Co-Ar, Co-Kr, and Co-Xe matrices which, after warm-up to 35-45 K, revert to the proposed tetracarbonyl, which is further supported by (b) matrix infrared $^{12}C^{16}O$-$^{13}C^{16}O$ and $^{12}C^{16}O$-$^{12}C^{18}O$ mixed isotopic substitution data, (c) the corresponding matrix Raman data in $^{12}C^{16}O$, (d) the matrix uv-visible data, and (e) the matrix ESR data.

Matrix Raman Experiments in Pure CO. The matrix Raman spectrum of the products of the cocondensation reaction of Co atoms and pure CO is shown in Figure 1B and 1C together with the matrix Raman depolarization mea-

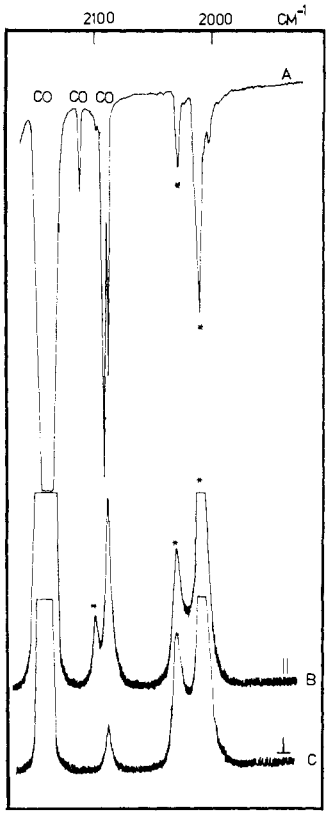

Figure 1. The matrix infrared (A) and Raman (B and C) spectra of $Co(CO)_4$ in a CO matrix at 6 K (the asterisks mark the CO stretching modes of $Co(CO)_4$). Parallel and crossed Raman polarization measurements are indicated by ∥ and ⊥, respectively.

surements. The complementary matrix infrared spectrum is included in Figure 1A for purposes of comparison.

Immediately apparent from these spectra are the infrared and Raman coincidences of the bands at 2028.8 and 2010.7 cm^{-1} and the appearance of a *new* Raman active band at 2107 cm^{-1}. The matrix Raman depolarization measurements (Figure 1B and 1C) show that the band at 2107 cm^{-1} is almost totally polarized, whereas the bands at 2028.8 and 2010.7 cm^{-1} are within experimental error depolarized, although a slight degree of polarization (less than 5%) might remain undetected. The existence of at least two CO stretching modes in the infrared spectrum tends to rule out an undistorted tetrahedral geometry for $Co(CO)_4$. Considering the two most likely distortions arising from a $^2T_2$ electronic ground state to be D_{2d} or C_{3v}, one expects the corresponding vibrational representations for CO stretching modes to be:

$$D_{2d} \text{ model: } \Gamma_{vib}{}^{\nu CO} = A_1 + B_2 + E$$

$$C_{3v} \text{ model: } \Gamma_{vib}{}^{\nu CO} = 2A_1 + E$$

If one examines the alternative vibrational assignments shown below then one is forced to base a C_{3v} conclusion on

	Activity		Polarization	
cm^{-1}	D_{2d}	C_{3v}	D_{2d}	C_{3v}
2107.0	R(A_1)	Ir/R(A_1)	pol	pol
2028.8	Ir/R(B_2)	Ir/R(A_1)	dep	pol
2010.7	Ir/R(E)	Ir/R(E)	dep	dep

(i) the observation of the infrared active, high frequency A_1 νCO stretching mode of the C_{3v} molecule, which is predicted to be weak and could be obscured by the $^{12}C^{18}O$-$^{13}C^{16}O$ (2092-2088 cm^{-1}) natural abundance isotopic bands and (ii) the observation of polarization on the low frequency

Table I. Matrix Infrared Data for the Binary Carbonyls of Cobalt in Various Matrices

Matrix	$CoCO^a$	$Co(CO)_2$	$Co(CO)_3$	$Co(CO)_4{}^c$
CO	*b*	*b*	*b*	2028.8, 2010.7
Xe	1947.0, 1941.0	1911.0	1971.0	2019.0, 2008.0
Kr	1952.0, 1944.0	1914.0	1977.0	2020.8, 2010.6
Ar	1956.0, 1949.0	1919.0	1982.0	2024.0, 2014.4
Ne	*d*	*d*	*d*	~2025.0, ~2015.0[e]

[a] Shows a matrix split (see text). [b] Can only be synthesized in dilute CO matrices. [c] $Co(CO)_4$ shows a doublet splitting of the νCO (T_2) mode in all matrices (see text). [d] Cannot be synthesized in Ne matrices at 8 K owing to the pronounced tendency of cobalt atoms to form the highest stoichiometry complex, binuclear compounds and higher cobalt clusters under these conditions. [e] These values are accurate only to ±2 cm^{-1} owing to the unavoidably large band widths of these modes in Ne matrices and the presence of clusters (see text).

(2028.8 cm^{-1}) totally symmetric A_1 νCO stretching mode of the C_{3v} molecule, which is, however, expected to be very slight because of "out-of-phase" vibrational coupling with the high frequency (2107.0 cm^{-1}) A_1 νCO mode.

Clearly it would be extremely unwise to make a structural decision on the basis of the above infrared and Raman data and one is forced to resort to other matrices, mixed isotope substitution, and ESR spectroscopy to help clarify the situation.

Infrared Experiments for $Co(CO)_4$ in Ne, Ar, Kr, and Xe Matrices. To establish whether or not the 18 cm^{-1} doublet splitting of the T_2 νCO stretching mode observed for $Co(CO)_4$ in CO matrices is reflecting a genuine distortion of the complex away from tetrahedral symmetry rather than simply a matrix effect originating in the low C_2 substitutional site symmetry of crystalline CO or a multiple trapping site effect, we decided to study $Co(CO)_4$ in a variety of isotropic noble gas matrices ranging from Ne through to Xe. Studies of this kind are of interest from the point of view of trying to clarify distortion ambiguities as well as seeking to evaluate the effect of the matrix environment on the infrared absorption frequencies of entrapped molecules.

In order to produce $Co(CO)_4$ in Ar, Kr, and Xe, cobalt atoms were cocondensed with CO/matrix ≃ 1/10 mixtures at 6 K (Figures 2 and 3). Under these conditions all four species $Co(CO)_n$ (where n = 1-4) were produced in varying amounts (described later) which, on warming to 30-40 K, slowly reverted to $Co(CO)_4$ (Figure 2). This procedure was found to be unnecessary for Ne/CO ≃ 1/10 matrices, as the lower rigidity and more pronounced surface diffusion on deposition in Ne favored the production of $Co(CO)_4$ even at 6-8 K.

The results of these studies are tabulated in Table I, from which two interesting observations become apparent. Firstly, the 18-cm^{-1} doublet splitting observed in CO matrices is retained yet substantially reduced in Ne, Ar, Kr, and Xe, indicating at this stage that the perturbation probably reflects a genuine distortion rather than a matrix site effect. Secondly, the components of the $Co(CO)_4$ doublet both experience a monotonically increasing blue frequency shift on passing from Xe through to Ne matrices.

In the context of the distortion problem we will continue to discuss the first point. The matrix-induced vibrational shifts, which are more pertinent to the theoretical treatment of matrix effects, will be considered in a later section.

Carbon Monoxide Mixed Isotopic Substitution Experiments; $^{12}C^{16}O$-$^{13}C^{16}O$ Matrix Infrared Data. When Co atoms were cocondensed with $^{12}C^{16}O$:$^{13}C^{16}O$ ≃ 1:1 mixtures ($Co:CO_{total}$ ≃ $1:10^5$), the matrix infrared spectrum shown in Figure 4 was obtained. The original doublet observed in the $^{12}C^{16}O$ experiment produced a total of *ten* re-

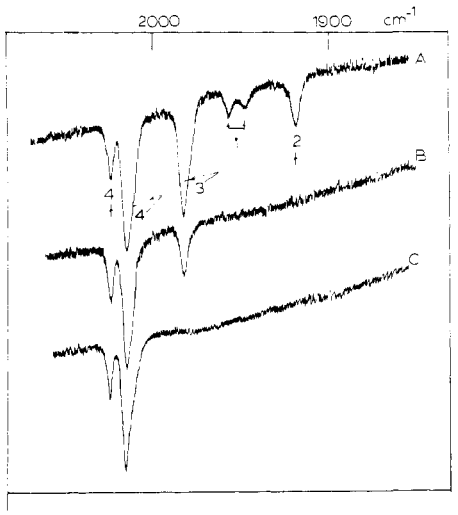

Figure 2. The matrix infrared spectrum of the products of the cocondensation reaction of Co atoms and CO/Ar ≃ 1/10 mixtures: (A) at 6 K; (B) and (C) after warming to 25 and 35 K, respectively (where 4 = $Co(CO)_4$, 3 = $Co(CO)_3$, 2 = $Co(CO)_2$, and 1 = Co(CO)).

Table II. Observed and Calculated Frequencies for $Co(^{12}C^{16}O)_n(^{13}C^{16}O)_{4-n}$ (where n = 0–4) C_{3v} Model

	Obsd (cm^{-1})	Calcd[a] (cm^{-1})	Symmetry assignment
Molecule (I)	2010.7	2010.5	E
$Co(^{12}C^{16}O)_4$	2028.8	2028.5	A_1
C_{3v}	2107.0	2107.0	A_1
Molecule (II)	1991.3	1990.9	A_1
$Co(^{12}C^{16}O)_3(^{13}C^{16}O)$	2010.7	2010.5	E
C_{3v}		2099.0	A_1
Molecule (III)	1974.6	1975.0	A'
$Co(^{12}C^{16}O)_3(^{13}C^{16}O)$	2026.4	2027.1	A'
C_s		2098.6	A'
	2010.7	2010.5	A''
Molecule (IV)	1986.8	1986.7	A'
$Co(^{12}C^{16}O)_2(^{13}C^{16}O)_2$	2024.6	2024.3	A'
C_s		2089.2	A'
	1965.7	1965.8	A''
Molecule (V)	1973.3	1973.2	A'
$Co(^{12}C^{16}O)_2(^{13}C^{16}O)_2$	1992.7	1992.9	A'
C_s		2089.1	A'
	2010.7	2010.5	A''
Molecule (VI)	1979.6	1979.6	A'
$Co(^{12}C^{16}O)(^{13}C^{16}O)_3$	1997.9	1997.9	A'
C_s	1965.7	1965.8	A''
		2077.1	A'
Molecule (VII)	1965.7	1965.8	E
$Co(^{12}C^{16}O)(^{13}C^{16}O)_3$	2010.7	2010.7	A_1
C_{3v}		2078.4	A_1
Molecule (VIII)	1965.7	1965.8	E
$Co(^{13}C^{16}O)_4$	*b*	1983.4	A_1
C_{3v}		2060.2	A_1

[a] The best fit force constants for the C_{3v} model were: k_r = 16.952, $k_{r'}$ = 16.755, $k_{rr'}$ = 0.328, and $k_{r'r'}$ = 0.425 mdyn/Å. After the final iteration the standard deviation was 0.611×10^{-5} which statistically represents a good fit, almost two orders of magnitude better than the D_{2d} model. [b] This frequency was observed by Rest et al. as a shoulder at 1983.6 cm^{-1}, in close agreement with our calculated value.

solvable isotopic frequencies in $^{12}C^{16}O$-$^{13}C^{16}O$, most of which are in reasonably close agreement with the isotopic data obtained in the same matrix environment by Rest et al.[7] As only five isotopic frequencies would be expected in this region for regular tetrahedral $Co(^{12}C^{16}O)_n(^{13}C^{16}O)_{4-n}$ (where n = 0–4; see for example the corresponding data for $Pd(CO)_4$ or $Pt(CO)_4$[13]), the mixed isotopic data support the contention that the molecule is somehow distorted away from regular tetrahedral.

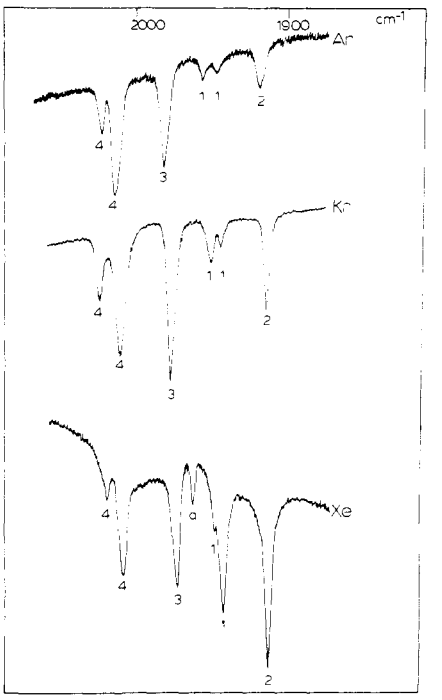

Figure 3. The matrix infrared spectra of the products of the cocondensation reaction of Co atoms and CO/Ar ≃ 1/10, CO/Kr ≃ 1/10, and CO/Xe ≃ 1/5 mixtures at 6 K ("a" is probably a matrix split of $Co(CO)_3$).

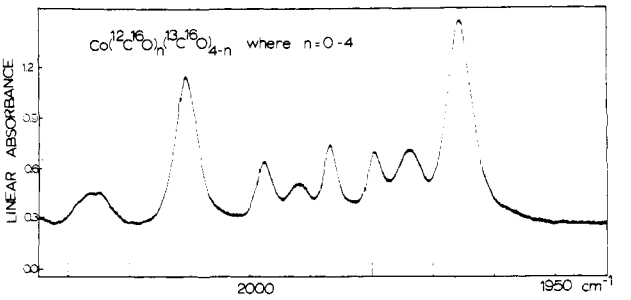

Figure 4. The matrix infrared spectrum of $Co(^{12}C^{16}O)_n(^{13}C^{16}O)_{4-n}$ (where n = 0–4) resulting from the cocondensation reaction of Co atoms with $^{12}C^{16}O/^{13}C^{16}O$ ≃ 45/55 mixtures at 6 K (where Co/CO ≃ $1/10^5$).

Frequency Calculations for C_{3v} and D_{2d} $Co(^{12}C^{16}O)_n(^{13}C^{16}O)_{4-n}$ (where n = 0–4) in CO Matrices. In order to distinguish between the two proposed distortions, frequency calculations were performed on the observed *ten*-line isotopic spectrum (in mixed $^{12}C^{16}O$-$^{13}C^{16}O$ matrices) assuming first C_{3v} and then D_{2d} symmetries, with the ultimate aim that one model would fit the data significantly better than the other.

As Rest et al.[7] only reported the results of the C_{3v} calculation and as our assignment of the distortion will inevitably lean heavily on the results of a least-squares analysis of the data for the C_{3v} and D_{2d} models, we will describe each calculation in turn.

The C_{3v} Model for $Co(CO)_4$. In the calculations, the Cotton-Kraihanzel force field approximation was employed.[16] As a result of $^{12}C^{16}O$-$^{13}C^{16}O$ isotopic substitution, the eight molecules listed in Table II need to be considered, where the four parameters k_r, $k_{r'}$, $k_{rr'}$, and $k_{r'r'}$ were adjusted to give the best fit for the C_{3v} model. The results of these calculations are shown in Table II.

The D_{2d} Model for $Co(CO)_4$. As a result of $^{12}C^{16}O$-$^{13}C^{16}O$ isotopic substitutions, the six molecules listed in

Table III. Observed and Calculated Frequencies for $Co(^{12}C^{16}O)_n(^{13}C^{16}O)_{4-n}$ (where $n = 0-4$) D_{2d} Model

	Obsd (cm^{-1})	Calcd[a] (cm^{-1})	Symmetry assignment
Molecule (I)	2010.7	2012.0	E
$Co(^{12}C^{16}O)_4$	2028.8	2026.6	B_2
D_{2d}	2107.0	2106.3	A_1
Molecule (II)	2010.7	2012.0	A''
$Co(^{12}C^{16}O)_3(^{13}C^{16}O)$	1979.6	1978.8	A'
C_s	2026.4	2022.8	A'
		2098.1	A'
Molecule (III)	1992.0	1993.9	A_1
$Co(^{12}C^{16}O)_2(^{13}C^{16}O)_2$		2089.1	A_1
C_{2v}	2010.7	2012.0	B_1
	1965.7	1967.5	B_2
Molecule (IV)	1973.3	1973.3	B
$Co(^{12}C^{16}O)_2(^{13}C^{16}O)_2$	2024.6	2020.5	B
C_2	1986.8	1984.4	A
		2088.2	A
Molecule (V)	1974.6	1975.1	A'
$Co(^{12}C^{16}O)(^{13}C^{16}O)_3$	1997.7	2001.8	A'
C_s		2076.8	A'
	1965.7	1967.5	A''
Molecule (VI)	1965.7	1967.3	E
$Co(^{13}C^{16}O)_4$		1981.6	B_2
D_{2d}		2059.5	A_1

[a] The best fit force constants for the D_{2d} model were $k_r = 16.806$, $k_{rr} = 0.452$, and $k_{rr'} = 0.333$ mdyn/Å. After the final iteration the standard deviation was 0.548×10^{-3} which statistically represents a poor fit.

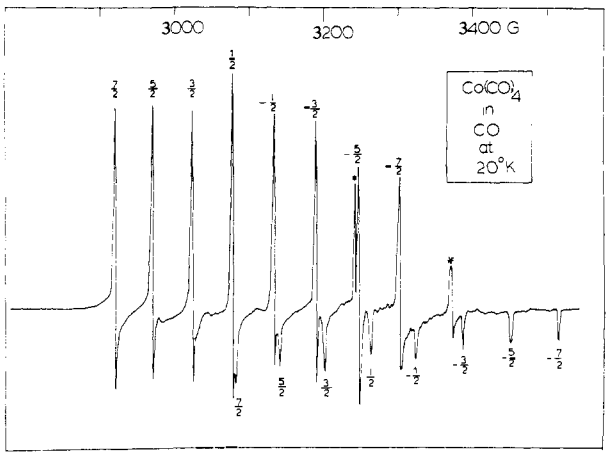

Figure 5. The matrix ESR spectrum of $Co(CO)_4$ resulting from the cocondensation reaction of Co atoms with CO at 6 K (impurity lines are indicated with an asterisk).

Table III need to be considered, where the three parameters k_r, k_{rr}, and $k_{rr'}$ were adjusted to give the best fit for the D_{2d} model. The results of these calculations are shown in Table III.

On comparing the calculated and observed frequencies and standard deviations for the C_{3v} and D_{2d} models, one finds consistently better agreement for the C_{3v} model. This parallels the findings of Rest et al.[7] Therefore, on the basis of the vibrational isotopic evidence, we propose that $Co(CO)_4$ experiences a C_{3v} trigonal distortion in CO matrices.

The Matrix ESR Spectrum of $Co(CO)_4$ in Solid CO. When Co atoms were cocondensed with CO onto a sapphire rod held at 6 K under conditions which favored the exclusive formation of $Co(CO)_4$ (see earlier section), the ESR spectrum displayed in Figure 5 was obtained. The close resemblance of this spectrum to the ESR spectrum previously obtained for the paramagnetic species formed on subliming $Co_2(CO)_8$ onto a 77 K cold finger[5] confirms that the sublimation route does indeed yield some $Co(CO)_4$ and not some other lower $Co(CO)_n$ carbonyl complex.

The ESR spectrum shown in Figure 5 is typical of a molecule having axial symmetry and $S = \frac{1}{2}$. The spin-Hamiltonian parameters found are

$$g_\parallel = 2.007 \pm 0.010$$

$$g_\perp = 2.128 \pm 0.010$$

$$A_\parallel(^{59}Co) = (58 \pm 1) \times 10^{-4}\ cm^{-1}$$

$$A_\perp(^{59}Co) = (55 \pm 1) \times 10^{4}\ cm^{-1}$$

(The large errors in g are due to the lack of a good frequency and magnetic field measurement capability in the Varian E-4 spectrometer.) These values are essentially the same as those reported for $Co(CO)_4$ in the $Co_2(CO)_8$ matrix.[4,5] The axial symmetry confirms the conclusions of ir and Raman analysis that $Co(CO)_4$ in a CO matrix is distorted from T_d symmetry.

In the previous analysis of the ESR spectrum by Fieldhouse et al.[5] it was assumed that the distortion was C_{3v} and that the distortion was large enough to make the energy difference between the first excited state and the ground state much larger than the spin-orbit interaction. In view of the preceding discussion of $Co(CO)_4$ in Ar and Kr matrices, it would seem necessary also to consider what ESR parameters would be expected for small distortions from tetrahedral symmetry. The equations for $g_\parallel$ and $g_\perp$ can be obtained by the same method used on the d^1 ion in an octahedral crystal field.[17] If we consider only the spin-orbit interaction among the t_2 orbitals, we obtain for the d^9 configuration in a tetrahedral field the equations

$$g_\parallel = 2.0023 \cos 2r - 2 \sin^2 r$$

$$g_\perp = 2.0023 \cos^2 r + \sqrt{2} \sin 2r$$

$$\tan 2r = \sqrt{2}/(\eta - \tfrac{1}{2})$$

$$\eta = \delta/\xi$$

for both C_{3v} and D_{2d} distortions. ξ is the one-electron spin-orbit interaction parameter and is always positive. δ is the energy difference, in the absence of spin-orbit coupling, between the e and a_1 orbitals for C_{3v} symmetry and the e and b_1 orbitals for D_{2d} symmetry. It is positive for an a, or b, ground state. The angle r takes values between 0 and 90°. Except for a couple of significant changes in sign, these equations are the same as for a d^1 ion in an octahedral field. There is one important difference, however, that needs mentioning because it has apparently been overlooked in theoretical treatments of this system. The spin-orbit interaction in the tetrahedral d^9 case splits the sixfold degenerate $^2T_2$ state into two states with the lower state being a twofold degenerate Kramer's doublet. Since this state cannot be further split by an electric field, it is not strictly correct to term a distortion from tetrahedral symmetry as a "Jahn-Teller distortion" as Burdett[18] has done.

Values of $g_\parallel$ and $g_\perp$ obtained from the above equations for various values of η are plotted in Figure 6. The equations give a negative value for $g_\parallel$ when η is between 1 and $-\infty$, but since experiment only gives the absolute values of g we have chosen to plot only absolute values in Figure 6. From the figure we see that $g_\parallel < g_\perp$ only when η is greater than zero, that is for the unpaired electron in a d_{z^2} orbital in a C_{3v} distortion or a $d_{x^2-y^2}$ orbital in a D_{2d} distortion. Further we deduce that it is unlikely that we are in the region where η is ~0 because $g_\parallel$ decreases, making it impossible to account for the fact that $g_\parallel \sim 2.0$ while $g_\perp$ is significantly greater than 2.0. Therefore we conclude that the ESR results can only be interpreted in terms of a large distortion as

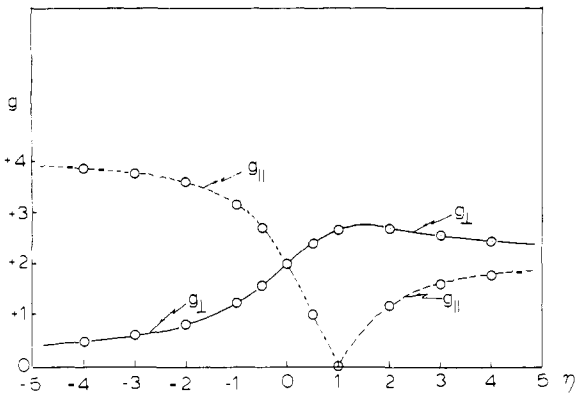

Figure 6. The dependence of $g_{\parallel}$ and $g_{\perp}$ on η (where $\eta = \delta/\xi$) for C_{3v} trigonal $Co(^{12}C^{16}O)_4$ (see text for notation).

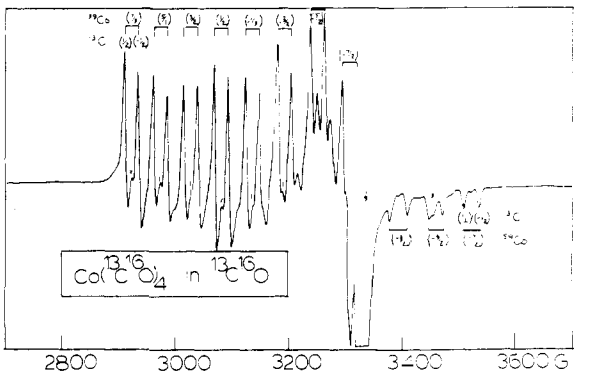

Figure 7. The matrix ESR spectrum of $Co(^{13}C^{16}O)_4$ resulting from the cocondensation reaction of Co atoms with 93% isotopically pure $^{13}C^{16}O$ at 6 K (asterisks indicate trace amounts of $Co(^{12}C^{16}O)_4$ arising from the residual 7% $^{12}C^{16}O$; arrows indicate impurity lines).

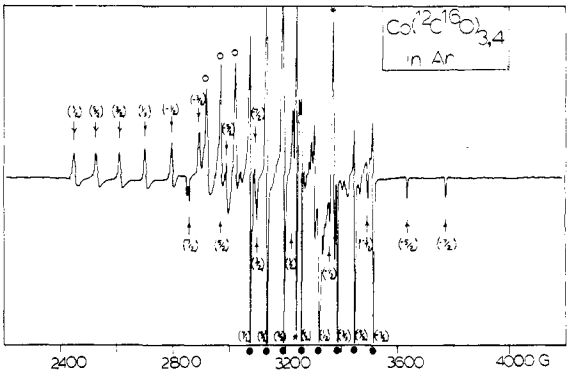

Figure 8. The matrix ESR spectrum of $Co(^{12}C^{16}O)_4$ and $Co(^{12}C^{16}O)_3$ resulting from the cocondensation of Co atoms with CO/Ar ≃ 1/10 mixtures at 10-12 K (the arrows indicate lines due to $Co(^{12}C^{16}O)_3$). The spectrum was recorded at 20 K for optimum resolution.

was done by Fieldhouse et al.[5] For a large distortion the spin-orbit terms arising from the excited ^2E states of T_d symmetry are as important as those coming from the $^2T_2$ states. For the d_{z^2} orbital of C_{3v} these terms contribute only to $g_{\perp}$, making it greater than 2.0 while for the $d_{x^2-y^2}$ orbital of D_{2d} they contribute only to $g_{\parallel}$, making it greater than 2.0. The only consistent explanation, therefore, of the g values for $Co(CO)_4$ in a CO matrix requires the assumption of a C_{3v} distortion which places the unpaired electron in the d_{z^2} orbital.

A striking confirmation of the C_{3v} distortion is obtained when the experiment is done using 93% $^{13}C^{16}O$. The ESR spectrum in this case is given in Figure 7 in which it will be noted that every line of Figure 5 is split into a doublet. Thus only one of the four ^{13}C nuclei about the Co atom has a significant hyperfine interaction. This would be expected for a d_{z^2} orbital in C_{3v} symmetry because only the CO group along the threefold symmetry axis would have a σ interaction between the 3d orbital of Co and a 2s orbital of the carbon atom. In D_{2d} symmetry all four ^{13}C nuclei would have to interact equally with the unpaired electron because all four CO ligands are made equivalent by the improper fourfold symmetry axis of D_{2d}.

The ^{13}C hyperfine constants are $A_{\parallel} = (26 \pm 2) \times 10^{-4}$ cm^{-1} and $A_{\perp} = (24 \pm 1) \times 10^{-4}$ cm^{-1}. It is of interest to compare these values with ^{13}C hyperfine values in similar systems. Wayland et al.[19] have reported values of $A_{\parallel} = 59.7$ and $A_{\perp} = 55.3 \times 10^{-4}$ cm^{-1} for a complex of CO with Co(II) tetraphenylporphyrin which also has one unpaired electron in a d_{z^2} orbital pointing towards the CO ligand. The σ interaction in $Co(CO)_4$ is apparently only half of that in the porphyrin complex. We can estimate the time spent by the unpaired electron on ^{13}C by use of the equations

$$A_{\parallel} = f_s A_{2s} + 2f_p A_{2p}$$

$$A_{\perp} = f_s A_{2s} - f_p A_{2p}$$

where A_{2s} is the hyperfine interaction of a carbon 2s electron, A_{2p} is the hyperfine interaction of a carbon 2p electron, and f_s and f_p are the fractions of time spent in each orbital. From Morton et al.[20] we find $A_{2s} = 1037 \times 10^{-4}$ cm^{-1} and $A_{2p} = 30.3 \times 10^{-4}$ cm^{-1}. Using these values we obtain $f_s = 0.024$ and $f_p = 0.02$ which means that the unpaired electron occupies an sp hybrid on carbon about 4-5%. In a similar manner we can obtain an estimate of time spent on the Co atom from the ^{59}Co hyperfine terms. For a d_{z^2} orbital

$$A_{\parallel} = K + P\left[\frac{4}{7} - \frac{1}{7}(g_{\perp} - 2.0023)\right]$$

$$A_{\perp} = K + P\left[-\frac{2}{7} + \frac{15}{14}(g_{\perp} - 2.0023)\right]$$

$$P = 2.0023 g_N \beta_e \beta_N \langle r^{-3} \rangle_{av}$$

Assuming that $A_{\parallel}$ is positive and $A_{\perp}$ negative, we obtain the values: $P = 162 \times 10^{-4}$ cm^{-1} and $K = -31 \times 10^{-4}$ cm^{-1}. K is the isotropic Fermi contact term and is normally about -90×10^{-4} cm^{-1} in cobalt[21] when no hybridization of 3d with 4s is allowed. Mixing of 4s makes a positive contribution to K so that the value found in $Co(CO)_4$ indicates a small amount of 4s hybridization. P would be expected to be ~200 cm^{-1} [21] for an unpaired electron in a free Co atom, hence our hyperfine data would have the unpaired electron spend ~80% of its time on the Co atom. The remaining 15% could be accounted for by assuming the electron spends ~5% of its time in the system of each of the three other carbonyl ligands.

From the preceding discussion it can be seen that a coherent and consistent explanation of the ESR results can be made for $Co(CO)_4$ in CO that supports the ir and Raman results. The story is much different, however, for the ESR spectra of $Co(CO)_4$ in an Ar matrix.

The Matrix ESR Spectrum for $Co(CO)_4$ in Solid Ar. When $Co(CO)_4$ is synthesized in Co/Ar ≃ 1/10 mixtures, the spectrum shown in Figure 8 results. The arrows indicate lines due to $Co(CO)_3$ whose spectrum will be discussed further on. After warming to 35 K to get rid of $Co(CO)_3$ and then cooling again, the spectrum in Figure 9 results in which we see that not only have the lines attributed to $Co(CO)_3$ disappeared but the appearance of the central

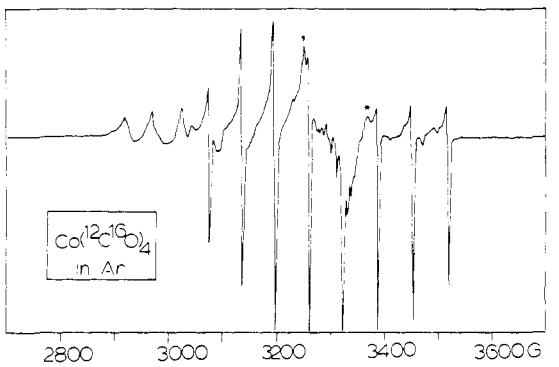

Figure 9. The same as Figure 8 but after annealing the matrix to 35 K, removing $Co(^{12}C^{16}O)_3$, and showing $Co(^{12}C^{16}O)_4$. The matrix was then recooled to 20 K for spectral recording.

portion of the spectrum has altered. Clearly there are at least two species present in addition to $Co(CO)_3$ whose relative amounts are altered in the annealing process. What is occurring becomes clearer when we study the ESR spectra for $Co(CO)_4$ in Ar using 93% $^{13}C^{16}O$. In Figure 10A is the spectrum obtained initially and Figure 10B shows the spectrum after annealing the sample. In the initial preparation there are two main species: $Co(CO)_3$ and what we will call $Co(CO)_4$ (I).

$Co(CO)_4$ (I) shows a hyperfine splitting from only one ^{13}C. As annealing progresses the $Co(CO)_3$ spectrum decreases and a new spectrum from a species which we will call $Co(CO)_4$ (II) increases from weak lines in Figure 10A to the dominant lines in Figure 10B. The lines from $Co(CO)_4$ (II) were not readily seen in Figures 8 and 9 because they overlap those of $Co(CO)_4$ (I) but they become evident after isotopic substitution since they exhibit a *triplet* pattern due to a hyperfine interaction with two ^{13}C nuclei.

Analysis of all spectra gives the following spin-Hamiltonian parameters for $Co(CO)_4$ (I) and (II).

$$Co(CO)_4 \text{ (I)}$$

$$g_{\parallel} = 2.132 \pm 0.010 \qquad g_{\perp} = 2.012 \pm 0.010$$

$$A_{\parallel}(^{59}Co) = (55 \pm 1) \times 10^{-4}\ cm^{-1} \qquad A_{\perp}(^{59}Co) = (59 \pm 1) \times 10^{-4}\ cm^{-1}$$

$$A_{\parallel}(^{13}C) = (24 \pm 1) \times 10^{-4}\ cm^{-1} \qquad A_{\perp}(^{13}C) = (25 \pm 1) \times 10^{-4}\ cm^{-1}$$

$$Co(CO)_4 \text{ (II)}$$

$$g_{\perp} = 2.014 \pm 0.010$$

$$A_{\perp}(^{59}Co) = (60 \pm 1) \times 10^{-4}\ cm^{-1}$$

$$A_{\perp}(^{13}C) = (27 \pm 1) \times 10^{-4}\ cm^{-1}$$

The parallel values for $Co(CO)_4$ (II) cannot be determined, but certainly $A_{\parallel}(^{59}Co)$ is less in magnitude than $A_{\perp}(^{59}Co)$ and probably $g_{\parallel} < g_{\perp}$.

At present we do not have a clear-cut explanation of these results. For $Co(CO)_4$ (I) the single ^{13}C interaction suggests C_{3v} symmetry with the one unpaired electron in a d_{z^2} orbital, but the g values contradict this. Having $g_{\parallel} > g_{\perp}$ is more suggestive of a $d_{x^2-y^2}$ orbital which is the ground state for D_{2d}, but the ^{13}C data contradict this. Further, the ^{13}C data for $Co(CO)_4$ (II) do not fit either a C_{3v} nor a D_{2d} distortion.

Of the two explanations which could be advanced for these results, one is chemically unacceptable in that it assumes three O-bonded CO groups in a C_{3v} $Co(CO)_4$ molecule. The second has some problems which make it difficult to accept without other supporting evidence. The second explanation would assume that species (I) has a C_{3v} distortion that makes the ^2E state the ground state rather than the $^2A_1$ state found in the CO matrix. This would simply involve a change in the angle θ to a value slightly greater than the tetrahedral angle in Ar rather than a value slightly less than tetrahedral in CO (see ref 22). Moreover it would assume that there is a further but smaller distortion such that

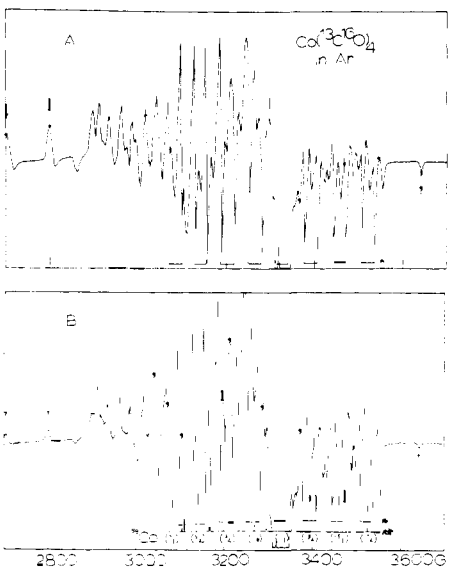

Figure 10. The matrix ESR spectrum of $Co(^{13}C^{16}O)_4$ and $Co(^{13}C^{16}O)_3$ resulting from the cocondensation of Co atoms with 93% isotopically pure $^{13}C^{16}O$ (a) at 10–12 K and (b) after annealing the matrix at 30–35 K. Arrows indicate some of the lines belonging to $Co(^{13}C^{16}O)_3$, single asterisks indicate some of the ^{13}C hyperfine lines belonging to $Co(^{13}C^{16}O)_4$ (I), and double asterisks $Co(^{13}C^{16}O)_4$ (II) (see text for notation). All spectra were recorded at 20 K for optimum resolution.

the unpaired electron is found in a d_{xz} type orbital which has one lobe pointing towards one CO molecule. To explain the observed axial symmetry of the resonance we must further assume this second distortion to be a dynamic Jahn-Teller type, in which it is equally probable for a given molecule that the d_{xz} orbital could be pointing towards any one of the three CO molecules disposed about the threefold symmetry axis. Assuming a rapid interconversion among the three distortions would average the x and y values of g and $A(^{59}Co)$, we can then account for the apparent axial symmetry.

In a like manner for species II, we can assume a major D_{2d} distortion which also gives rise to a ^2E ground state (this is possible for a value of the dihedral angle τ slightly less than tetrahedral; see ref 22) and then a smaller distortion to a ground state in which the unpaired electron is in a d_{xz} type orbital. In D_{2d} symmetry, however, a d_{xz} orbital has its two lobes pointing at two different CO molecules and hence the spectrum would show the observed triplet pattern. Again a dynamic Jahn-Teller type distortion would explain the apparent axial symmetry in the ESR spectrum. This explanation is most appealing but it requires assumptions that are difficult to accept. The distortion that splits the ^2E state must be large enough to make the energy difference between the d_{xz} and d_{yz} orbitals large compared to the spin-orbit parameter ξ (which is $\sim$390 cm^{-1} for the free Co atom[23]) to have the ground state be essentially d_{xz} or d_{yz} and to have g values close to 2.0. At the same time the potential barrier to going from one distortion to the next must be small enough to allow rapid interconversion at temperatures as low as 6 K, which is the lowest temperature that can be reached in the present apparatus.

If this second explanation were true, the results would support the contention of Burdett[18] and Hoffmann[22] that the D_{2d} distortion is more stable than the C_{3v} by a small amount, since it is the D_{2d} species that increases during the annealing process. It does not, however, support their conclusion that the ground state orbital is $d_{x^2-y^2}$.

Matrix Uv–Visible Experiments for $Co(CO)_4$ in CO. Electronic absorption phenomena of metal carbonyl complexes

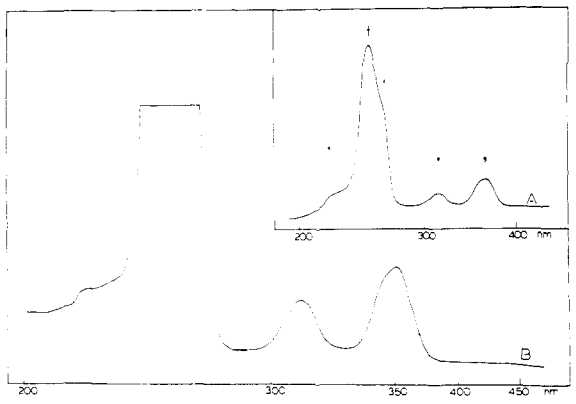

Figure 11. The matrix uv-visible spectrum of $Co(CO)_4$ resulting from the cocondensation reactions of Co atoms with CO at 6 K: (A) 5-min deposition and (B) further deposition. (Arrows indicate absorptions associated with $Co(CO)_4$.)

have recently been reviewed.[24] Generally, the complexes exhibit a number of intense transitions in the uv-visible region which are associated with ligand field and M → L and L → M charge transfer absorptions.

When $Co(CO)_4$ was synthesized from the cocondensation of Co atoms with pure CO matrices at 6 K, the uv-visible spectrum shown in Figure 11 was obtained. The spectrum basically consists of four main lines, two medium intense lines at low energies (28090 cm^{-1}, showing a slight splitting, and 31650 cm^{-1}) with an intense line at higher energies centered at 38610 cm^{-1} with a shoulder at about 36900 cm^{-1}.

In the interpretation of the gross features of this spectrum we will consider the molecular orbital scheme for a d^9 tetrahedral complex that has undergone a trigonal distortion along the z axis shown below. To aid our assignment of

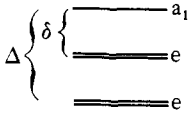

the optical spectrum of $Co(CO)_4$ we will rest heavily on what is known about the related system $Ni(CO)_4$.[25]

Nickel tetracarbonyl has a d^{10} electronic configuration and has a regular tetrahedral geometry. The absorption spectrum shows an intense band centered at about 48550 cm^{-1} with shoulders at approximately 44500 and 42270 cm^{-1}. These transitions have been assigned to excitations of electrons in the T_2 and E levels of the metal-to-ligand localized orbitals.[25] Trigonal $Co(CO)_4$ with a d^9 electronic configuration would therefore be expected to show, in addition to the related metal-to-ligand charge transfer transitions (shifted to slightly lower energies in $Co(CO)_4$ compared to $Ni(CO)_4$ because of the lower valence orbital ionization energies of the cobalt metal d orbitals compared to the corresponding molecule orbitals), a single ligand field transition corresponding to excitation of an electron from the E ground state to the A_1 excited state. (From the ESR data we estimate a lower limit for $\delta \simeq 5850$ cm^{-1}. Hence the transition from the upper E level to the A_1 level is not expected to appear within the range of our spectrometer (190-700 nm).)

With this in mind we propose that the high energy bands observed at 39120 and 37110 cm^{-1} are cobalt-to-CO charge transfer transitions, analogous to those observed in the range 48550-42270 cm^{-1} for $Ni(CO)_4$.[25] Of the remaining bands observed at lower energies, one is most probably the expected $^2E \rightarrow {}^2A_1$ d-d transition (Table IV).

Table IV. The Uv–Visible Spectra for $Co(CO)_4$ in CO and Ar Matrices

CO matrix (cm^{-1})	Ar matrix (cm^{-1})	Tentative assignment
28090 m 28820 wsh	29410 mbr	$^2E \leftarrow {}^2A_1$
31650 mw	32790 wsh 33780 m	C.T.
37110 msh	39600 msh	C.T.
39120 vs	41670 vs	C.T.

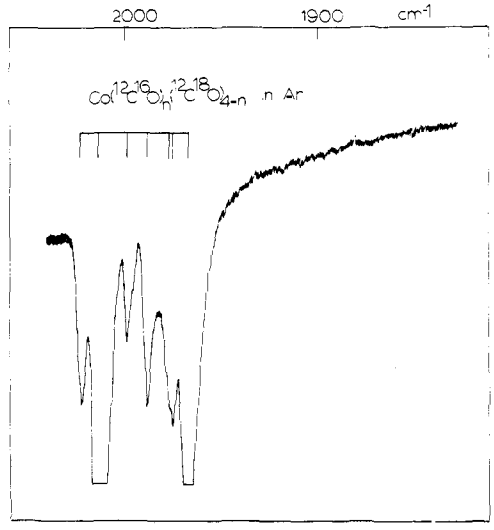

Figure 12. The matrix infrared spectrum of $Co(^{12}C^{16}O)_n(^{12}C^{18}O)_{4-n}$ in Ar (where n = 0-4) resulting from the cocondensation reaction of Co atoms with $^{12}C^{16}O/^{12}C^{18}O/Ar \simeq 1/1/20$ mixtures at 6 K after warming to 35-40 K.

The uv-visible spectrum for $Co(CO)_4$ was also recorded in CO-Ar matrices. Apart from blue frequency shifts on all observed lines, the gross features of the spectrum closely resembled those observed for $Co(CO)_4$ in CO (Table IV).

$^{12}C^{16}O$–$^{12}C^{18}O$–Ar and $^{12}C^{16}O$–$^{12}C^{18}O$–Kr Matrix Infrared Data. Using techniques similar to those described earlier for producing $Co(CO)_4$ in dilute Ar and Kr matrices, analogous reactions were performed in dilute $^{12}C^{16}O$-$^{12}C^{18}O$-Ar and $^{12}C^{16}O$-$^{12}C^{18}O$-Kr matrices. After warm-up to 35-40 K, the isotopic spectrum of $Co(^{12}C^{16}O)_n(^{12}C^{18}O)_{4-n}$ (where n = 0-4) could be easily observed (Figure 12 and Tables V and VI). Apart from small matrix frequency shifts on passing from Ar to Kr, these spectra were essentially identical (Tables V and VI). Besides the expected doublet splitting of the $Co(^{12}C^{16}O)_4$ and $Co(^{12}C^{18}O)_4$ molecules, the remaining mixed isotopic molecules in Ar and Kr appear to display at most *three* other lines compared to *six* for pure carbon monoxide mixed isotopic matrices, and as such resemble the mixed isotopic spectra observed for regular tetrahedral tetracarbonyls.[13]

At this stage it is worth noting that the doublet splitting of $Co(CO)_4$ in CO matrices (18 cm^{-1}) is significantly larger than that observed for the molecule in Ne (10 cm^{-1}), Ar (9.6 cm^{-1}), Kr (10.2 cm^{-1}), and Xe (11.0 cm^{-1}) matrices which are themselves larger than the 6-7 cm^{-1} "matrix site splittings" observed for the regular tetrahedral d^{10} tetracarbonyls $M(CO)_4$ (where M = Ni, Pd, or Pt) in solid CO.[13] The implication is therefore that $Co(CO)_4$ is distorted away from regular tetrahedral in all of the matrices studied, the larger splitting in CO probably arising from a combination of a "matrix site splitting" (ca. 6-7 cm^{-1}) superimposed on a small but genuine "distortion splitting" (ca. 10 cm^{-1}; see ESR section described later for details of the distortion)

Table V. Calculated and Observed Frequencies for $Co(^{12}C^{16}O)_n(^{12}C^{18}O)_{4-n}$ (where n = 0–4) in Ar Matrices

Obsd (cm^{-1})	Calcd[a] (cm^{-1})	C_{3v} Model (I) Assignment
1967.0	1967.2	E (VIII), E (VII), A" (VI), A" (IV)
1974.5	1971.6	A' (V)
	1974.6	A' (VI)
	1974.8	A' (III)
1977.0	1976.2	A_1 (VIII)
1987.5	1984.3	A' (IV)
	1985.4	A' (V)
	1989.4	A_1 (II)
1997.5	1997.4	A' (VI)
	1998.7	A_1 (VII)
2013.5	2015.7	E (I), E (II), A" (III), A" (V)
2023.0	2021.8	A'(IV)
	2023.9	A' (III)
	2025.0	A_1 (I)
	2033.4	A_1 (VIII)
	2053.7	A' (VI)
	2060.1	A_1 (VII)
	2065.1	A' (V)
	2068.9	A' (IV)
	2074.0	A_1 (II)
	2076.7	A' (III)
	2083.7	A_1 (I)

[a] The best fit C–K force constants for the C_{3v} model are k_r = 16.879, $k_{r'}$ = 16.685, $k_{rr'}$ = 0.262, and $k_{r'r'}$ = 0.270 mdyn/Å (see text and Table III for notation).

Table VI. Calculated and Observed Frequencies for $Co(^{12}C^{16}O)_n(^{12}C^{18}O)_{4-n}$ (where n = 0–4) in Ar Matrices

Obsd (cm^{-1})	Calcd[a] (cm^{-1})	D_{2d} Model (II) Assignment
1967.0	1968.3	E (VI), A" (V), B_2 (III)
1974.5	1971.6	B (IV)
	1972.7	A' (V)
	1975.5	B_2 (VI)
1977.0	1977.5	A' (II)
	1983.9	A (IV)
1987.5	1990.3	A_1 (III)
1997.5	1997.4	A' (V)
2013.5	2016.9	E (I), A" (II), B_1 (III)
2023.0	2020.9	B (IV)
	2022.0	A' (II)
	2024.2	B_2 (I)
	2029.4	A_1 (VI)
	2052.1	A' (V)
	2063.1	A (IV)
	2064.0	A_1 (III)
	2072.1	A' (II)
	2079.5	A_1 (I)

[a] The best fit C–K force constants for the D_{2d} model are k_r = 16.723, k_{rr} = 0.289, and $k_{rr'}$ = 0.229 mdyn/Å (see text and Table IV for notations).

which essentially accounts for the observed doublet splitting of 18 cm^{-1}.

Frequency Calculations for $Co(^{12}C^{16}O)_n(^{12}C^{18}O)_{4-n}$ (where n = 0–4) in Ar. In the light of the ESR data for $Co(CO)_4$ in Ar, we will treat the corresponding infrared isotopic data in terms of a mixture of C_{3v} $Co(CO)_4$ (I) and D_{2d} $Co(CO)_4$ (II) isomers as discussed earlier.

To test this idea, we have computed the isotopic spectra of $Co(^{12}C^{16}O)_n(^{12}C^{18}O)_{4-n}$ (where n = 0–4) in both C_{3v} and D_{2d} symmetries with two stringent restrictions. Firstly the doublet splitting observed for the molecules $Co(^{12}C^{16}O)_4$ and $Co(^{12}C^{18}O)_4$ was retained in the calculations. Secondly the lines belonging to the mixed isotopic molecules n = 1–3 were collapsed (accidental coincidences) to a *triplet* (Figure 12) rather than a *sextet* (Figure 4) as observed in CO. With these constraints, a least-squares analysis was performed on the observed isotopic spectrum of $Co(^{12}C^{16}O)_n(^{12}C^{18}O)_{4-n}$ in Ar matrices.

Considering that the bandwidths at half-height of the observed isotopic lines were between 4 and 8 cm^{-1}, it can be seen from Tables V and VI that both molecules (C_{3v} $Co(CO)_4$ (I) and D_{2d} $Co(CO)_4$ (II)) yield equally acceptable fits between the calculated and observed isotopic frequencies (Tables V and VI). It is therefore not inconceivable that molecules I and II observed in the ESR spectrum of $Co(CO)_4$ in Ar are in fact the C_{3v} and D_{2d} isomers of $Co(CO)_4$, indistinguishable from our vibrational isotope patterns and optical spectra, yet easily discernible from their ESR magnetic parameters and ^{13}C hyperfine splittings.

Intermediate Binary Carbonyls of Cobalt, $Co(CO)_n$ (where n = 1–3). Having established the identity of $Co(CO)_4$ and the conditions which minimize the formation of binuclear species, it proved to be a relatively simple matter to synthesize and characterize the intermediate carbonyls $Co(CO)_n$ by variable concentration, matrix dependence, matrix warm-up, and isotopic substitution experiments. In many respects the behavior of $Co(CO)_n$ resembled very closely the related complexes $Ni(CO)_n$ (where n = 1–4).[13] The following experiments were performed.

When Co atoms were cocondensed with $^{12}C^{16}O/Ar \simeq 1/1000$ a single sharp absorption was observed at 1954.5 cm^{-1}. In the analogous $^{12}C^{16}O/^{13}C^{16}O/Ar \simeq 1/1/2000$ experiment, a doublet was observed at 1954.5 and 1910.2 cm^{-1}, confirming that the absorbing species can be assigned to CoCO. The calculated and observed shifts are in excellent agreement and yield a Cotton-Kraihanzel force constant of 15.40 mdyn/Å. The monocarbonyl absorption was particularly sensitive to matrix concentration and deposition conditions (temperature and rate of deposition). For example, in more concentrated Ar-CO matrices the monocarbonyl appeared as a matrix split doublet (1956/1949 cm^{-1}, confirmed by mixed isotopic substitution) which underwent a red shift on passing to Kr-CO (1952.0/1944.0 cm^{-1}) and to Xe (1947.0/1941.0 cm^{-1}) matrices.

When Co atoms were cocondensed with more concentrated matrices, for example $CO/Kr \simeq 1/50$, three main νCO absorptions were observed, the most intense being the monocarbonyl with two other lines at 1914 and 1977 cm^{-1}, the latter being the least intense (Figure 13A). On warming these matrices to 20 K, the line at 1977 cm^{-1} begins to grow in together with the appearance of a band at 2011 cm^{-1} (Figure 13B and 13C), the latter being the most intense line of $Co(CO)_4$ in Kr matrices. At 35–40 K the tetracarbonyl absorptions are most prominent (2021/2011 cm^{-1}), the other three having almost disappeared. The data described above serve to establish the presence of four binary cobalt carbonyl species whose warm-up behavior suggests the following a priori assignment: $Co(CO)_4$, 2021/2011 cm^{-1}; $Co(CO)_3$, 1977 cm^{-1}; $Co(CO)_2$, 1914 cm^{-1}; Co(CO), 1952/1944 cm^{-1}; a frequency assignment paralleling that previously reported for $Ni(CO)_n$ (where n = 1–4).[13b]

Additional support for these assignments originates from two other kinds of experiment. Firstly, when Co atoms were cocondensed with CO/Ar, CO/Kr, and $CO/Xe \simeq 1/10$ matrices at 6 K, the infrared spectra shown in Figures 3A–C and Table I were observed. The similarities and differences to the previously described $Kr/CO \simeq 1/50$ experiment (Figure 13) are quite apparent. First, the tetracarbonyl absorption as expected is far more prominent in the more concentrated 1/10 matrices (It is worth noting that when

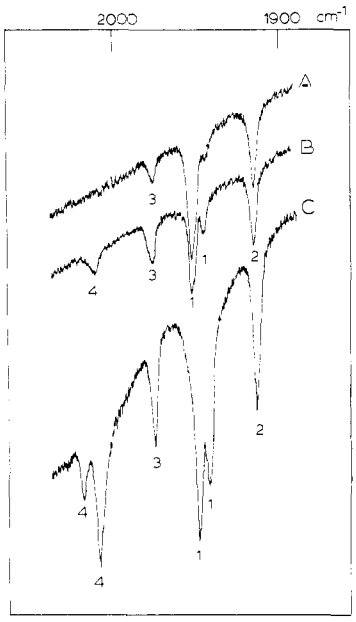

Figure 13. The matrix infrared spectrum of the products of the cocondensation reaction of Co atoms with CO/Kr ≃ 1/50 mixtures: (A) at 6 K, (B) and (C) after warm-up to 20 and 30 K showing $Co(CO)_n$ (where n = 1-4).

the analogous experiments were performed with 20 K depositions, the only species formed was $Co(CO)_4$.) and second, the relative intensities of the four species vary on passing from Ar to Kr to Xe matrices in the order (discussed later) $I_4 > I_3 > I_2 > I_1$ in Ar/CO ≃ 1/10, $I_3 > I_4 \simeq I_2 > I_1$ in Kr/CO ≃ 1/10, $I_2 > I_1 > I_3 \simeq I_4$ in Xe/CO ≃ 1/5.

The warm-up behavior of the four species is quite unambiguous, the previously identified monocarbonyl first decreasing in intensity, followed by the absorption at 1919 cm^{-1} (Ar), 1914 cm^{-1} (Kr), and 1911 cm^{-1} (Xe). At about 20-30 K in Ar matrices, the tetracarbonyl predominates, the only other absorbing species being at 1982 cm^{-1} (Figure 2). A similar situation prevails at about 45-50 K in Kr and Xe matrices which identifies $Co(CO)_3$ at 1982, 1976, and 1971 cm^{-1} and $Co(CO)_2$ at 1919, 1914, and 1911 cm^{-1} in Ar, Kr, and Xe matrices, respectively. Confirmation of these vibrational assignments stems from the mixed isotopic substitution experiments to be described.

Intermediate Binary Carbonyls of Cobalt; $^{12}C^{16}O$-$^{12}C^{18}O$-Kr and $^{12}C^{16}O$-$^{12}C^{18}O$-Ar Mixed Isotope Experiments. It remains to confirm the assignments of the absorptions suspected to belong to the di- and tricarbonyl of cobalt. This was achieved by cocondensing Co atoms with $^{12}C^{16}O/^{12}C^{18}O/Kr$ ≃ 1/1/20 mixtures at 6 K. A typical infrared spectrum obtained *on deposition* is shown in Figure 14A from which the isotopic components of the mono-, di-, and tricarbonyl can be easily identified. Only *trace* amounts of the tetracarbonyl are apparent at this stage of the experiment. The anomalously high intensity of the 1914.0-cm^{-1} line of $Co(^{12}C^{16}O)_2$ arises from an accidental overlap with $Co(^{12}C^{18}O)$. On warming the matrix to 25-30 K, the isotopic lines of the tetracarbonyl can be seen to grow in and from the changes in absorbances of the remaining lines the isotopic spectra of $Co(^{12}C^{16}O)_p(^{12}C^{18}O)_{3-p}$ (where p = 0-3) and $Co(^{12}C^{16}O)_q(^{12}C^{18}O)_{2-q}$ (where q = 0-2) can be identified (Figure 14B and Table VII). The analogous experiments performed in $^{12}C^{16}O/^{12}C^{18}O/Ar$ ≃ 1/1/40 matrices, apart from small matrix shifts (4-6 cm^{-1}), are essentially the same as those obtained in Kr matrices (Table VII) and thereby provide additional support for the di- and tricarbonyl vibrational assignments.

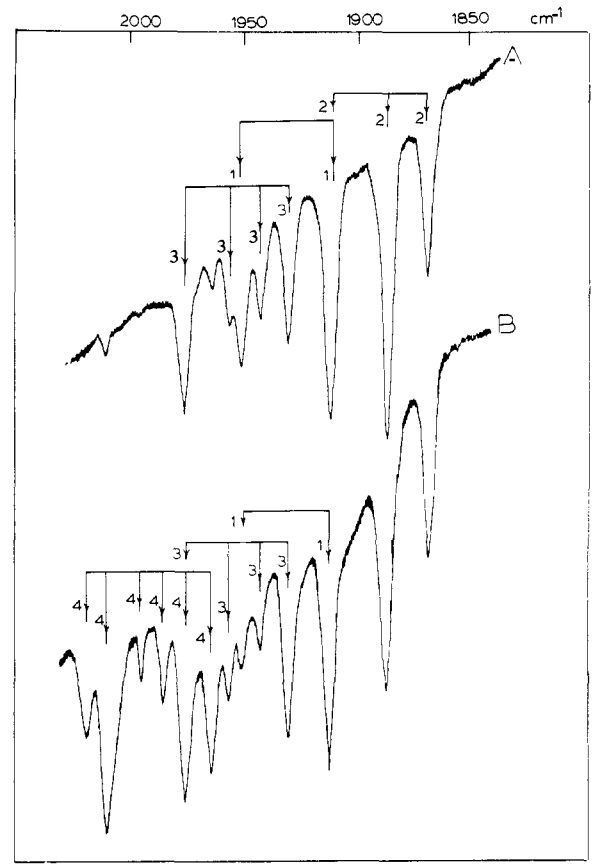

Figure 14. The matrix infrared spectrum of the products of the cocondensation reaction of Co atoms with $^{12}C^{16}O/^{12}C^{18}O/Kr$ ≃ 1/1/20 mixtures: (A) at 6 K and (B) after warm-up to 25-30 K showing $Co(^{12}C^{16}O)_n(^{12}C^{18}O)_{m-n}$ (where m = 4, n = 0-4; m = 3, n = 0-3; m = 2, n = 0-2; and m = 1, n = 0-1).

Table VII. Calculated and Observed Frequencies for $Co(^{12}C^{16}O)_p(^{12}C^{18}O)_{3-p}$ and $Co(^{12}C^{16}O)_q(^{12}C^{18}O)_{2-q}$ in Argon and Krypton Matrices (where p = 0-3 and q = 0-2)

Obsd (cm^{-1}) $^{12}C^{16}O/^{12}C^{18}O/$ Ar (1/1/40)	Calcd (cm^{-1})[a]	Obsd (cm^{-1}) $^{12}C^{16}O/^{12}C^{18}O/$ Kr (1/1/20)	Calcd (cm^{-1})[b]	Assignment
1982.5	1983.5	1977.0	1978.2	$Co(^{12}C^{16}O)_3$
1962.5	1962.9	1957.0	1957.5	$Co(^{12}C^{16}O)(^{12}C^{18}O)_2$
1948.5	1947.9	1943.5	1942.7	$Co(^{12}C^{16}O)_2(^{12}C^{18}O)$
1936.5	1935.7	1931.5	1930.5	$Co(^{12}C^{18}O)_3$
1919.5	1920.6	1914.0	1914.7	$Co(^{12}C^{16}O)_2$
1893.5	1893.5	1888.0	1888.0	$Co(^{12}C^{16}O)(^{12}C^{18}O)$
1875.5	1874.3	1870.5	1868.6	$Co(^{12}C^{18}O)_2$

[a] The best fit force constants for $Co(CO)_3$ in Ar are k_{CO} = 16.61 and $k_{CO\cdot CO}$ = 0.71 mdyn/Å and for $Co(CO)_2$ are k_{CO} = 16.05 and $k_{CO\cdot CO}$ = 1.15 mdyn/Å. [b] The best fit force constants for $Co(CO)_3$ in Kr are k_{CO} = 16.50 and $k_{CO\cdot CO}$ = 0.69 mdyn/Å and for $Co(CO)_2$ are k_{CO} = 16.05 and $k_{CO\cdot CO}$ = 1.24 mdyn/Å.

The ESR Spectrum of $Co(CO)_3$ in Ar. The spectrum indicated by arrows in Figures 8 and 10 is attributed to $Co(CO)_3$ by reason of its appearance and disappearance under conditions analogous for the infrared bands. It is a typical S = ½ axially symmetric resonance with spin-Hamiltonian parameters of $g_\parallel$ = 2.002 ± 0.010, $g_\perp$ = 2.394 ± 0.010, $A_\parallel(^{59}Co)$ = (125 ± 1) × 10^{-4} cm^{-1}, and $A_\perp(^{59}Co)$ = (106 ± 1) × 10^{-4} cm^{-1}. Surprisingly no ^{13}C hyperfine is observed as can be seen in Figure 10. It is estimated that any ^{13}C hyperfine interaction must be less than 2 × 10^{-4}

cm^{-1} because the line widths in $Co(^{13}C^{16}O)_3$ are not much different from those for $Co(^{12}C^{16}O)_3$.

The axial symmetry is consistent with a C_{3v} or D_{3h} symmetry, and the g values are only consistent with the unpaired electron being in a d_{z^2} orbital. The absence of ^{13}C hyperfine is inconsistent with D_{3h} symmetry because a σ interaction should occur between the d_{z^2} orbital and the 2s orbitals of carbon giving rise to a measurable splitting of the resonances into a quartet pattern. It can be estimated from the splitting of $Co(CO)_4$ in CO that this splitting should be about 8×10^{-4} cm^{-1} assuming a comparable σ interaction. If there were a considerable distortion from the planar structure of D_{3h} into a C_{3v} symmetry (infrared intensity calculations show that the totally symmetric A_1 νCO stretching mode could pass undetected for an angular distortion anywhere between 0 and 10° from planarity; for example, when $\theta = 95°$, $I_E/I_{A_1} \simeq 130$; when $\theta = 100°$, $I_E/I_{A_1} \simeq 32$), the σ interaction between the d_{z^2} orbital and the carbon 2s orbitals would be greatly reduced, just as observed for the three CO's in $Co(CO)_4$ in CO.

There is, however, a problem with this interpretation which must be mentioned. If we analyze the ^{59}Co hyperfine terms in the same manner as we did $Co(CO)_4$ in CO we obtain the values of $P = 50 \times 10^{-4}$ cm^{-1} and $K = 99 \times 10^{-4}$ cm^{-1} for both $A_\parallel$ and $A_\perp$ being positive and $P = 606 \times 10^{-4}$ cm^{-1} and $K = -187 \times 10^{-4}$ cm^{-1} for $A_\parallel$ positive and $A_\perp$ negative. The second set of values is obviously not correct because P is much too large but the other set gives a value of P that would predict that the unpaired electron is on the Co atom only 25% of the time. If the electron is 75% on the CO ligands, even in the π system, we would expect a measurable ^{13}C hyperfine pattern to be seen. It is not readily apparent how one can resolve these contradictions.

Frequency Calculations for $Co(^{12}C^{16}O)_p(^{12}C^{18}O)_{3-p}$ and $Co(^{12}C^{16}O)_q(^{12}C^{18}O)_{2-q}$ (where p = 0–3 and q = 0–2). The isotopic spectra of cobalt tricarbonyl and cobalt dicarbonyl and the infrared *inactivity* of the totally symmetric CO stretching mode for each molecule indicate regular D_{3h} and $D_{\infty h}$ geometries, respectively. The axial symmetry properties displayed in the ESR spectrum of $Co(CO)_3$ (Figures 8 and 10) together with the nonobservation of ^{13}C hyperfine splitting are, however, more consistent with a C_{3v} trigonal pyramidal assignment. As mentioned earlier, a *small* distortion of about 10° away from planarity could have passed undetected in the infrared spectrum. With this in mind, least-squares analyses were performed on (i) the observed *four*-line isotopic spectra of $Co(^{12}C^{16}O)_p(^{12}C^{18}O)_{3-p}$ in Ar and Kr (where p = 0–3) and (ii) the observed *three*-line isotopic spectra of $Co(^{12}C^{16}O)_q(^{12}C^{18}O)_{2-q}$ in Ar and Kr (where q = 0–2). The two parameters k_{CO} and $k_{CO,CO}$ were adjusted to give the best fit frequencies for the di- and tricarbonyl. The results are listed in Table VII together with the best fit force constants. The agreement between the observed and calculated frequencies was acceptable for all lines and provides convincing support for the validity of our vibrational assignments.

Metal–Ligand Stretching Modes. As is often found to be the case for matrix-isolated binary carbonyls, the observation and assignment of lines in the metal–ligand stretching region of the infrared spectrum (600–200 cm^{-1}) are problematical because of their low absorbance coefficients compared to the relatively high values of the corresponding CO stretching modes. The binary cobalt carbonyls were no exception in this respect. Very weak absorptions in the low frequency region could be observed for $Co(CO)_4$ at 552 and 486 cm^{-1} only when the CO stretching mode at 2010.7 cm^{-1} was fully absorbing. By analogy with $Ni(CO)_4$, we assign the higher frequency line at 552 cm^{-1} to the $\delta CoCO$ mode and the lower frequency line at 486 cm^{-1} to the νCo-C mode (cf. 459 and 423 cm^{-1}, respectively, in $Ni(CO)_4$). To obtain a value for the M–C bond stretching force constant for $Co(CO)_4$ with the present data is not possible. However, we can estimate the k_{CoC} by considering $Co(CO)_4$ to be approximated by tetrahedral CoX_4 (where X is equal to the mass of CO) and by using the equation

$$\lambda_{T_2} = k_{CoC}(\mu_X + \tfrac{4}{3}\mu_{Co})$$

where μ_X and μ_{Co} are the reciprocal masses of $^{12}C^{16}O$ and Co, respectively. The values obtained by this method for $Co(CO)_4$ and $Ni(CO)_4$ are $k_{NiC} = 1.80$ and $k_{CoC} = 2.42$ mdyn/Å. Note that $k_{CoC} > k_{NiC}$ which is the inverse of the order found for the respective C–K k_{CO} values. These and other force constant trends are discussed in a later section.

Co–CO Reactions at High Cobalt Concentrations; Binuclear Complex Formation. When the cocondensation reactions of Co atoms and pure $^{12}C^{16}O$ (or $^{12}C^{16}O/Ar \simeq 1/10$) matrices are performed at Co:CO $\simeq 1:10^3$, at which concentrations the statistical generation of binuclear complexes should be of the order of 1% of the mononuclear complexes, complicated infrared spectra are obtained (Figure 15B). In the light of our earlier studies with binuclear complex formation in matrix cocondensation reactions,[11,14] several features of the above results are worthy of discussion.

Figure 15A shows the infrared spectrum for an authentic sample of $Co_2(CO)_8$ vaporized at 30°C and isolated in an Ar matrix at about $1:10^3$. Absorptions assignable to both the cobalt–cobalt bonded and CO-bridge bonded isomers can be identified. By comparing the data for $Co(CO)_4$ (Figure 15C) and $Co_2(CO)_8$ (Figure 15A) with the data for the $Co/CO \simeq 1/10^3$ reaction (Figure 15B and Table VIII), it can be seen that appreciable concentrations of both $Co(CO)_4$ and $Co_2(CO)_8$ (both isomers) are formed in the latter reaction. Moreover, detectable quantities of $Co_2(CO)_n$ (where $n < 8$) are also formed under these conditions as seen from the broad absorption in the region of 1941 cm^{-1}. As described previously, binuclear species can arise in the matrix in two ways. The first is statistical and the second is through reactions in the surface region of the matrix during the first few moments following deposition and before the kinetic energy of the reagents has been accommodated, hence while the molecules are still fairly mobile. In the case of the Co–CO reaction, our data clearly indicate that the surface reaction pathway far exceeds in importance the statistical generation of dimers. Only by reducing the Co:CO ratio to values less than $1:10^4$ is it possible to obtain an infrared spectrum showing mainly $Co(CO)_4$ (Figure 15C). By contrast, at Co:CO $\simeq 1:10^2$ the infrared spectrum shows mainly $Co_2(CO)_8$.

The matrix material also plays an important role in metal atom cocondensation reactions. For example, in Ne matrices the infrared spectra showed the presence of $Co(CO)_4$, $Co_2(CO)_8$ (both isomers), some unidentified $Co_2(CO)_n$ complexes (where $n < 8$), and trace amounts of CO chemisorbed on small Co clusters (as seen by a broad shoulder at about 2000 cm^{-1} on the low frequency side of the $Co(CO)_4$ absorption[15]) but no traces of $Co(CO)_n$ (where n = 1, 2, or 3). These results clearly indicate the highly mobile nature and poor quenching ability of Ne matrices for metal atom cocondensation reactions even at 6–8 K. Note that the absence of the lower carbonyls $Co(CO)_n$ (where n = 1–3) in $CO/Ne \simeq 1/10$ matrices represents the extreme case of the trend described earlier for Ar/CO, Kr/CO, and Xe/CO $\simeq$ 1/10 matrices (Figure 3) where the higher carbonyls are favored in the order Ne > Ar > Kr > Xe. The presence of large quantities of binuclear cobalt complexes in Ne matrices supports the contention that bimolecular processes of the type

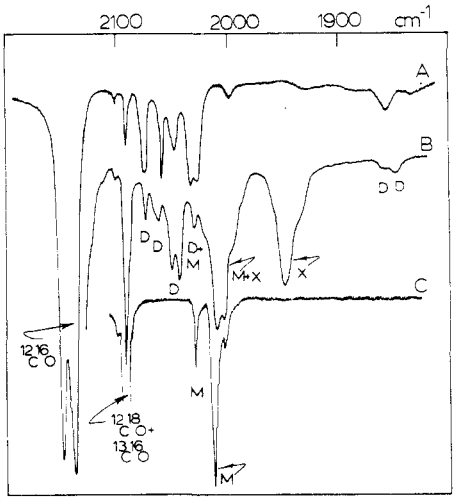

Figure 15. The infrared spectrum of (A) $Co_2(CO)_8$ in Ar (approximately 1:1000), (B) and (C) the infrared spectra of the products of the cocondensation reaction of Co atoms with CO at Co:CO ≃ $1:10^3$ and Co:CO ≃ $1:10^5$ showing the presence of $Co(CO)_4$ (M) and $Co_2(CO)_8$ (D), respectively. (The lines marked × probably belong to $Co_2(CO)_n$ species, where $n < 8$ and/or higher aggregates $Co_x(CO)_y$—see text.)

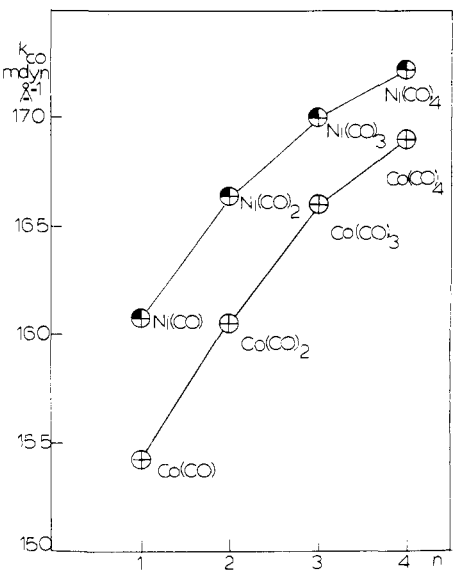

Figure 16. Graphical representation of the Cotton-Kraihanzel CO bond stretching force constants for $M(CO)_n$ (where M = Ni or Co) as a function of the coordination number n = 1-4.

Table VIII. Matrix Infrared Spectrum of the Products of the Co–CO–Ar Cocondensation Reaction under Conditions Which Favor Binuclears, Compared to the Infrared Spectrum of $Co_2(CO)_8$ Matrix Isolated in Solid Argon

Co/CO/Ar (1/100/1000) 15 K (this study)	$Co_2(CO)_8$/Ar (1/1000) 15 K (this study)	$Co_2(CO)_8$ (CO bridge bonded isomer) (ref 15)	$Co_2(CO)_8$ (metal–metal bonded isomer) (ref 15)	Assignment[a]
2074 m	2074 s	2071 vs		D_b
2064 m	2059 s		2069 vs	D_t
2048 s	2048 sh	2044 vs		D_b
2044 s	2046 m	2042 vs		D_b
2030 m	2032 s		2031 ms	D_t
2022 m	2027 s		2022 vs	D_t
2014 vs				$Co(CO)_4$
2004 sh[b]				$CO_2(CO)_n$
1998 sh[b]				$Co_2(CO)_n$
1950 s[b]				$Co_2(CO)_n$
1860 sh	1864 sh	1866 sh		D_b
1846 w	1855 w	1857 s		D_b

[a] D_b = CO bridge bonded isomer of $Co_2(CO)_8$; D_t = metal–metal bonded isomer of $Co_2(CO)_8$. [b] Metal concentration and warm-up experiments suggest that these absorptions belong to a binuclear carbonyl $Co_2(CO)_n$ (where $n < 8$).

$$Co(CO)_n + Co(CO)_m \rightarrow Co_2(CO)_{n+m}$$

$$Co(CO)_n + Co \rightarrow Co_2(CO)_n$$

$$Co_2 + CO \rightarrow Co_2(CO) \rightarrow \text{etc.}$$

are *favored* pathways in the most highly mobile, least polarizable matrices.

Discussion of Results

Having characterized all of the binary carbonyls of cobalt $Co(CO)_n$ (where n = 1-4), it is of considerable interest to examine trends in their force constants, bonding properties, and molecular and electronic structures.

Force Constant Trends. The best fit Cotton-Kraihanzel force constants for $Co(CO)_n$ together with the analogous data for $Ni(CO)_n$, summarized graphically in Figure 16 and listed in Table IX, display an interesting parallel trend

Table IX. Best Fit Cotton–Kraihanzel CO Stretching Force Constants for the Binary Carbonyls of Cobalt, $Co(CO)_n$ (where n = 1–4)

Molecule[a]	k_{CO}	$k_{CO \cdot CO}$	$k_{CO'}$[b]	$k_{CO' \cdot CO'}$[b]
$Co(CO)_4$ in CO	16.95	0.43	16.76	0.33
$Co(CO)_4$ in Ar	16.88	0.26	16.69	0.27
$Co(CO)_3$ in Ar	16.61	0.71		
$Co(CO)_3$ in Kr	16.50	0.69		
$Co(CO)_2$ in Ar	16.05	1.15		
$Co(CO)_2$ in Kr	16.05	1.24		
Co(CO) in Ar	15.40			
Co(CO) in Kr	15.33			
Co(CO) in Xe	15.27			

[a] The best fit force constants derived for Ar, Kr, and Xe matrices refer to the frequencies observed in 1/10 to 1/20 CO/matrix ratios. [b] Apply only to the C_{3v} calculation for $Co(CO)_4$ in CO matrices.

in which the k_{CO} values for the cobalt series are all smaller than the corresponding values of the nickel series. For the tetracarbonyls $Co(CO)_4$ and $Ni(CO)_4$ an inverse trend is found for the k_{MC} values.

The trend observed for the k_{CO} values on passing from group 7b to 8b $M(CO)_n$ complexes (assumed to be roughly isostructural for n = 1-4) is not unexpected, as the d-orbital stabilities increase in the same order. This would result in decreased d_π-π^* back-bonding from the metal to the CO ligands, with a concomitant increase in the σ charge donation from the 5σ molecular orbital of the CO to the appropriate symmetry orbital of the metal. Both of these processes would have the overall effect of strengthening the CO bond(s), a prediction which parallels the observed trend on passing from the $Co(CO)_n$ to the $Ni(CO)_n$ group of complexes. The corresponding effect on the M-C bond(s) is not so easily rationalized, as the σ- and π-effects oppose each other and one can only conclude after the fact that the decrease in M-C π-bonding outweighs the increase in M-C σ-bonding, consistent with the observation that $k_{CoC} > k_{NiC}$ for $Co(CO)_4$ and $Ni(CO)_4$, respectively.

A final point worth mentioning is the larger value of k_{CO} for $Co(CO)_4$ compared to k_{CO} for $Co(CO)_4^-$,[26] a trend reflecting the placement of an extra electron in the d-valence shell of the anion, with an accompanying increase in the extent of d_π-π^* back-bonding and decrease in CO to Co

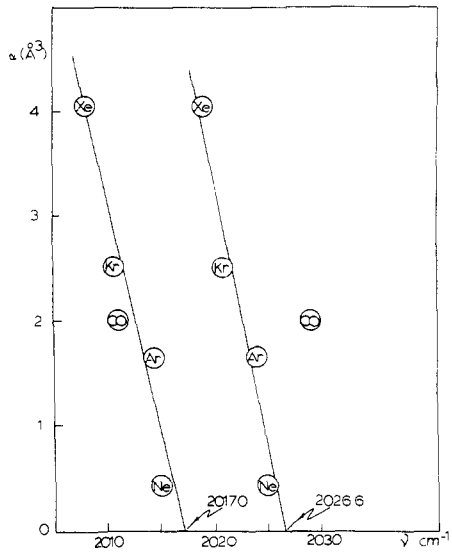

Figure 17. Polarizability (α, Å^3) frequency (ν, cm^{-1}) plot for the *two* CO stretching modes of $Co(CO)_4$ in Xe, Kr, Ar, Ne, and CO matrices. (Estimated gas phase frequencies are obtained by extrapolation to α = 0; see text.)

σ-bonding. As expected, this effect is even more pronounced when $Co(CO)_4$ is compared with $Fe(CO)_4^{2-}$.[27]

Complex	k_{CO}, mdyn/Å	Complex	k_{CO}, mdyn/Å
$Ni(CO)_4$	17.26	$Co(CO)_4^-$	13.22
$Co(CO)_4$	16.88	$Fe(CO)_4^{2-}$	11.40

Vibrational Frequency Shifts for $Co(CO)_n$ in Various Matrices. The theoretical treatment of matrix environmental effects, which can result in shifts or splittings of spectral bands of trapped species, is a complicated problem even for atomic and diatomic molecules.[28] A detailed evaluation of a vibrational shift from the gas phase to the matrix, defined as $\Delta\nu = \nu_{gas} - \nu_{matrix}$, involves the determination of inductive, dispersive, and repulsive contributions to $\Delta\nu$, which in all but the simplest of systems is extremely complex and makes quantitative evaluation of matrix shifts impracticable.

In principle, the theories put forward to account for nonspecific solvent shifts should be applicable to the related problem of solutes in matrices, the main difference being a flexible solvent cage for solutions but a "rigid" cavity for matrices.

Let us assume that the difference between the above situations is slight and that we can apply the Buckingham equation,[29] shown below,

$$\Delta\nu/\nu = C_1 + \tfrac{1}{2}(C_2 + C_3)\left(\frac{\epsilon' - 1}{2\epsilon' + 1}\right)$$

originally put forward to explain nonspecific solvent shifts for a solute molecule in a flexible solvent cage, to the present case of $Co(CO)_n$ molecules in nonpolar, noble gas matrices.

Having examined $Co(CO)_n$ (where n = 1-4) in a variety of matrices, it is of interest to note a definite trend that is apparent in their matrix vibrational frequencies. Without exception, the CO stretching frequencies for each complex show a red shift (a loose cage environment, according to Pimentel and Charles[30]) on passing from Ar to Kr to Xe matrices. The corresponding frequencies as expected show an approximately linear dependence on matrix polarizability (see for example $Co(CO)_4$ in Figure 17). An extrapolation of these linear plots of zero polarizability yields what we shall term "estimated gas phase frequencies" for $Co(CO)_n$ (where n = 1-4) listed in Table X. Using these estimated values of ν_{gas} one can determine the Buckingham frequency shifts $\Delta\nu/\nu$ (where $\Delta\nu = \nu_{gas} - \nu_{matrix}$ and ν is taken as the arithmetic mean of ν_{gas} and ν_{matrix}). These are plotted as a function of $(\epsilon' - 1)/(2\epsilon' + 1)$ for Ar, Kr, and Xe matrices in Figure 18.

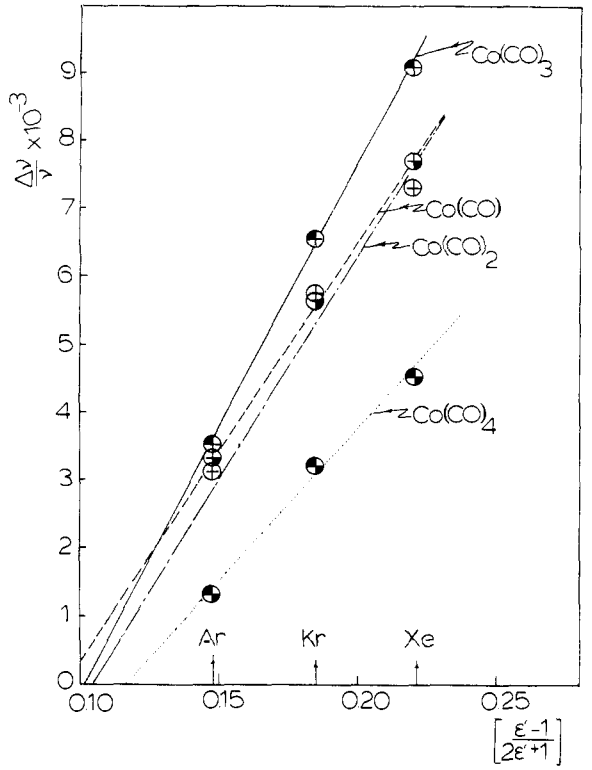

Figure 18. Buckingham plots for $Co(CO)_n$ (where n = 1-4) in Ar, Kr, and Xe matrices (see text for notation).

Table X. Buckingham Frequency Plots for $Co(CO)_n$ (where n = 1-4) in Ar, Kr, and Xe Matrices at 20 K

		ν_{matrix}[a]	$\Delta\nu$	$(\Delta\nu/\nu \times 10^{-3})$[c]	$(\epsilon' - 1)/(2\epsilon' + 1)$[d]
$Co(CO)_4$	Ar	2014.4	2.6	1.290	0.148
	Kr	2010.6	6.4	3.178	0.185
	Xe	2008.0	9.0	4.472	0.221
	Gas[b]	2017.0			
$Co(CO)_3$	Ar	1982.0	7.0	3.526	0.148
	Kr	1976.0	13.0	6.557	0.185
	Xe	1971.0	18.0	9.091	0.221
	Gas[b]	1989.0			
$Co(CO)_2$	Ar	1919.0	6.0	3.122	0.148
	Kr	1914.0	11.0	5.731	0.185
	Xe	1911.0	14.0	7.299	0.221
	Gas[b]	1925.0			
Co(CO)	Ar	1952.5	6.5	3.324	0.148
	Kr	1948.0	11.0	5.631	0.185
	Xe	1944.0	15.0	7.686	0.221
	Gas[b]	1959.0			

[a] Frequencies observed at 1/10 matrix ratios in all cases. [b] Extrapolated value. [c] ν is the arithmetic mean frequency observed for the complex in the matrix and gas phase. [d] $\epsilon'_{20\,K}$ = 2.19 (Xe), 1.88 (Kr), and 1.63 (Ar).

The predicted linear dependence of $\Delta\nu/\nu$ vs. $(\epsilon' - 1)/(2\epsilon' + 1)$ on the basis of Buckingham's equation appears to hold well for all $Co(CO)_n$ species (where n = 1-4) although the data can only be tested for Ar, Kr, and Xe matrices because of the limited ϵ' (20 K) data available for solid state gases at low temperatures.

Although the results are not extensive, it would appear that the noble gases give approximately linear Buckingham plots and as such suggest that the observed frequency shifts

Table XI. Predicted and Observed Geometries for $M(CO)_n$ Species (where n = 4 and 3)

	$V(CO)_4$	$Cr(CO)_4$	$Mn(CO)_4$	$Fe(CO)_4$	$Co(CO)_4$	$Ni(CO)_4$	$Co(CO)_4^-$
Calcd geo	$C_{2v}{}^{a-c}$	$C_{2v}{}^{a-d}$	$C_{2v}{}^{a,c,e}$ $D_{4h}{}^{b-d}$	$D_{2d}{}^{a}$ $D_{4h}{}^{b-d}$ $C_{2v}{}^{c,e}$	$D_{2d}{}^{a-c}$	$T_d{}^{a,b}$	
Obsd geo	*f*	C_{2v}	*f*	C_{2v}	C_{3v}, D_{2d}	T_d	
Ref	32	33		34	7 and this study	26	

	$V(CO)_3$	$Cr(CO)_3$	$Mn(CO)_3$	$Fe(CO)_3$	$Co(CO)_3$	$Ni(CO)_3$	$Cu(CO)_3$ $Ni(CO)_3^-$
Calcd geo	$C_{3v}{}^{a-d}$ $D_{3h}{}^{b,c,e}$	$C_{3v}{}^{a,b,d}$ $D_{3h}{}^{b,e}$ $C_{2v}{}^{c,e}$	$C_{3v}{}^{a}$ $C_{2v}{}^{b-d}$ $D_{3h}{}^{b,e}$	$C_{2v}{}^{a-d}$ $C_{3v}{}^{b,e}$	$C_{3v}{}^{a}$ $C_{2v}{}^{b,c}$	$C_{3v}{}^{a}$ $D_{3h}{}^{b}$	
Obsd geo	C_{3v} or D_{3h}	C_{3v}	*f*	C_{3v}	C_{3v}	D_{3h}	D_{3h}
Ref	32	33		35	This study	36	37, 38

[a] Hoffmann orbital-based calculation. [b] Burdett's MIE calculation. [c] Jahn–Teller considerations. [d] Low spin. [e] High spin. [f] Geometries not yet established.

for $Co(CO)_n$ most probably originate from nonspecific solute matrix interactions rather than "weak chemical bonds" between the complexes and the matrix as recently found for $Cr(CO)_5\cdots X$[31] (where X = Ne, Ar, Kr, Xe, CO, SF_6, CH_4, or CF_4).

As a final point we would like to draw particular attention to the "parallel" behavior exhibited in the polarizability-frequency plots of the *two* components of the CO stretching mode of $Co(CO)_4$ in Ne, Ar, Kr, and Xe matrices (Figure 17). Extrapolation of these data to zero polarizability yields a "gas phase splitting" of ca. 9.6 cm^{-1} and a convincing demonstration of a genuine molecular distortion for $Co(CO)_4$ rather than just a matrix perturbation.

In this context we note the anomalous position for CO in Figure 17 which is entirely consistent with our earlier proposal that the larger splitting observed for $Co(CO)_4$ in solid CO arises from a combination of a "matrix site splitting" (ca. 6-7 cm^{-1}) superimposed on a small but genuine "molecular distortion splitting" (ca. 10 cm^{-1}).

Molecular Distortions Arising from Electronic Effects. The Structures of Binary Transition Metal Carbonyl Fragments $M(CO)_n$ (where n = 4 and 3). The object of this discussion is to try to provide a unified view of the geometries of $M(CO)_n$ fragments (where n = 4 and 3) in the light of recent experimental results and MO calculations.[18,22] We will restrict our discussions to metal atoms of the first transition series. The calculations on which molecular geometry conclusions have been based were generally of the extended Huckel type with minimum internal energy criteria. The fragment geometries that have been explored theoretically can be considered to be derived from an octahedron by successive stripping away of one CO, followed by a sequence of geometrical rearrangements of the remaining $M(CO)_n$ fragment. For each fragment a range of geometrical distortions was explored. As it turns out, Hoffmann's orbital-based results[22] lead to the same general conclusions as Burdett's orbital-overlap and Jahn-Teller arguments[18] with some exceptions. It should be noted that a knowledge of level ordering is a prerequisite for application of Jahn-Teller considerations, whereas the direct orbital approach of Hoffmann carries information not only on level ordering but also on geometrical trends and reactivities of the various molecules and, as such, seems to be more widely applicable.

Up to the time of writing, the $M(CO)_n$ (where n = 4 and 3) binary carbonyls which have been synthesized and for which structural information is essentially complete are listed in Table XI.

General Considerations. If one surveys the structural data for $M(CO)_n$ species presented in Table XI, several points are worthy of discussion. Let us briefly examine n = 4 and 3 in turn.

General Considerations. If one surveys the structural data for $M(CO)_n$ species presented in Table XI, several points are worthy of discussion. Let us briefly examine n = 4 and 3 in turn.

Tetracarbonyls. Because of the large number of possible configurations of a tetracarbonyl fragment (T_d, D_{2d}, C_{4v}, and C_{2v}), several slices through the many-dimensional potential energy surface of $M(CO)_4$ had to be examined in detail in order to make meaningful deductions concerning the geometrical preferences of various d-electron configurations.[22] The predictions for d^6 $Cr(CO)_4$ and d^{10} $Ni(CO)_4$ agree well with the experimental data. The d^9 $Co(CO)_4$ molecule presents an interesting problem as both Hoffmann and Burdett give a D_{2d} structure as the most stable form. Experimentally, there now appears to be general agreement that $Co(CO)_4$ in CO matrices adopts a C_{3v} configuration. However, in CO-Ar matrices it is quite likely that C_{3v} and D_{2d} isomers coexist with the D_{2d} form being slightly more stable. This is not totally unexpected in view of the separate local minimum of slightly higher energy calculated for the C_{3v} structure.[22]

There seems to be some disagreement regarding the stable configuration of low-spin d^8 $Fe(CO)_4$. Hoffmann prefers the D_{2d} structure, whereas Burdett favors the D_{4h} structure. As it turns out in practice, $Fe(CO)_4$ has been assigned a C_{2v} structure and is suspected to be a high-spin complex.[34]

Tricarbonyls. The calculated optimum geometries for $M(CO)_3$ fragments shown in Table XI reveal some minor discrepancies. Somewhat unexpectedly, Hoffmann's calculations for the d^{10} $M(CO)_3$ species favor a C_{3v} geometry (an almost flat pyramid, $\theta \simeq 98°$) which is computed to be about 1 kcal/mol lower in energy than the D_{3h} trigonal planar structure.[22] However, all known tricoordinate d^{10} $M(CO)_3$ (where M = Ni, Pd, and Pt) species appear to be trigonal planar.[13] In this context a cautionary reminder is necessary. The planarity (or nonplanarity) of $M(CO)_3$ species (D_{3h} or C_{3v}) is usually determined by the nonobservation (or observation) of the totally symmetric CO stretching vibration in the infrared spectrum. This, however, can be an extremely tenuous exercise as, for a near planar structure, the symmetric CO stretching vibration is expected to be extremely weak compared to its asymmetric counterpart vibration and may pass undetected in the infrared spectrum, even though isotopic data and Raman data can help pinpoint the position of this mode.

This situation has been experienced in the present study with the vibrational data for $Co(CO)_3$ which favored the D_{3h} geometry for the molecule. Only with the aid of the ESR spectrum was it possible to establish the C_{3v} pyramidal nature of $Co(CO)_3$.

For the remaining carbonyls, d^6 $Cr(CO)_3$ and d^8 $Fe(CO)_3$, there seems to be general agreement that the low-spin C_{3v} geometry is the stable form of $Cr(CO)_3$. The ob-

served C_{3v} geometry of $Fe(CO)_3$ would appear to suggest that $Fe(CO)_3$ is a high-spin species.[35]

The interesting $d^{10}s^1$ species $Cu(CO)_3$, $Ag(CO)_3$, and $Ni(CO)_3^-$ have recently been synthesized and without exception appear to be planar molecules.[37-39] These geometries are consistent with the suggestion that interactions with a spherically symmetrical s orbital do not affect the geometry of these species.[18]

In conclusion, it is clear that Kettle's earlier suggestion[40] that simple $M(CO)_n$ species should adopt the highest symmetry structures is no longer valid. Although there is still not complete agreement between Hoffmann's and Burdett's calculations, it is clear from the results obtained so far that the unusual and sometimes unexpected geometries adopted by binary carbonyl complexes are electronic in origin. Hopefully the few discrepancies which still prevail will be clarified and a logical scheme will emerge.

Acknowledgments. We would like to thank Dr. Martin Moskovits for many helpful and stimulating discussions, Mr. Alex Campbell, Mr. Karl Molnar, Mr. Bob Torbet, and Mr. Martin Mittelstaedt for technical assistance, the National Research Council of Canada, the Research Corporation, the Atkinson Foundation and Liquid Carbonic for financial assistance, and the National Research Council for a scholarship (for L.A.H.).

References and Notes

(1) L. Mond, H. Hirtz, and M. D. Cowap, *J. Chem. Soc.*, **97**, 798 (1910).
(2) D. T. Thompson and R. Whyman in "Transition Metals in Homogeneous Catalysis", G. N. Schrauzer, Ed., Marcel Dekker, New York, N.Y., 1971.
(3) A. J. Chalk and J. F. Harrod, *Adv. Organomet. Chem.*, **6**, 119 (1968); R. Whyman, *J. Organomet. Chem.*, **81**, 97 (1974).
(4) H. J. Keller and H. Wawersik, *Z. Naturforsch.*, **206**, 938 (1965).
(5) S. A. Fieldhouse, B. W. Fullam, G. W. Nellson, and M. C. R. Symons, *J. Chem. Soc., Dalton Trans.*, 567 (1974).
(6) D. R. Bidinosti and N. S. McIntyre, *Chem. Commun.*, 1 (1967).
(7) O. Crichton, M. Poliakoff, A. J. Rest, and J. J. Turner, *J. Chem. Soc., Dalton Trans.*, 1321 (1973).
(8) (a) M. Moskovits and G. A. Ozin, paper given at the International Raman Conference, Reims, 1972; (b) G. A. Ozin in "Vibrational Spectra of Trapped Species", H. Hallam, Ed., Wiley, London, 1973.
(9) E. P. Kündig, M. Moskovits, and G. A. Ozin, *J. Mol. Struct.*, **14**, 137 (1972).
(10) M. Moskovits and G. A. Ozin, *J. Appl. Spectrosc.*, **26**, 481 (1972).
(11) L. Hanlan and G. A. Ozin, *J. Am. Chem. Soc.*, **96**, 6324 (1974).
(12) H. Huber and G. A. Ozin, unpublished work.
(13) (a) E. P. Kündig, D. McIntosh, M. Moskovits, and G. A. Ozin, *J. Am. Chem. Soc.*, **95**, 7234 (1973); (b) R. DeKock, *Inorg. Chem.*, **10**, 1205 (1971); (c) J. H. Darling and J. S. Ogden, *ibid.*, **11**, 666 (1972); (d) E. P. Kündig, M. Moskovits, and G. A. Ozin, *Can. J. Chem.*, **50**, 3587 (1972); *J. Mol. Struct.*, **14**, 137 (1972).
(14) (a) G. A. Ozin, "Transition Metal Atoms in the Synthesis of Binuclear Complexes", paper given at Merck Symposium "Metal Atoms in Chemical Synthesis", Seehelm, 1974; E. P. Kündig and M. Moskovits, *Angew. Chem., Int. Ed. Engl.*, **14**, 292 (1975); (b) H. Huber, E. P. Kündig, G. A. Ozin, and A. J. Poë, *J. Am. Chem. Soc.*, **97**, 308 (1975); (c) E. P. Kündig, M. Moskovits, and G. A. Ozin, *ibid.*, **97**, 2097 (1975). (Note that ref 14c deals with $Cu-Cu_2$ matrix reactions with CO.)
(15) G. Blyholder and M. C. Allen, *J. Am. Chem. Soc.*, **91**, 3158 (1969); K. Noack, *Spectrochim. Acta*, **19**, 1925 (1963); G. Bor, *ibid.*, **19**, 2065 (1963).
(16) F. A. Cotton and C. S. Kraihanzel, *J. Am. Chem. Soc.*, **84**, 4432 (1962).
(17) B. R. McGarvey, "Transition Metal Chemistry", Vol. 3, R. L. Carlin, Ed., Marcel Dekker, New York, N.Y., 1966, pp 89–201.
(18) J. K. Burdett, *J. Chem. Soc., Faraday Trans., 2*, **70**, 1599 (1974).
(19) B. B. Wayland, J. U. Minkiewixz, and M. E. Abd-Elmageed, *J. Am. Chem. Soc.*, **96**, 2795 (1974).
(20) J. R. Morton, J. R. Rowlands and D. H. Whiffen, *Nat. Phys. Lab. (U.K.), Rep*, **BPR 13** (1962).
(21) B. R. McGarvey, *J. Phys. Chem.*, **71**, 51 (1967).
(22) M. Elian and R. Hoffmann, *Inorg. Chem.*, **14**, 1058 (1975).
(23) B. H. Figgis, "Introduction to Ligand Fields", Interscience, New York, N.Y., 1966, p 60.
(24) M. Wrighton, *Chem. Rev.* **74**, 401 (1974).
(25) A. F. Schreiner and T. L. Brown, *J. Am. Chem. Soc.*, **90**, 3366 (1968).
(26) E. W. Abel, *Q. Rev., Chem. Soc.*, **17**, 133 (1963).
(27) H. Stammereich, *J. Chem. Phys.*, **32**, 1482 (1960).
(28) A. J. Barnes in "Vibrational Spectra of Trapped Species", H. Hallam, Ed., Wiley, London, 1973.
(29) A. D. Buckingham, *Proc. R. Soc. London, Ser. A*, **248**, 169 (1958); *ibid.*, **255**, 32 (1960); *Trans. Faraday Soc.*, **56**, 753 (1960).
(30) G. C. Pimentel and S. W. Charles, *Pure Appl. Chem.*, **7**, 111 (1963).
(31) J. J. Turner and R. N. Perutz, private communication and *J. Am. Chem. Soc.*, in press.
(32) L. A. Hanlan, H. Huber and G. A. Ozin, *Inorg. Chem.*, submitted for publication.
(33) J. J. Turner, private communication and *J. Am. Chem. Soc.*, in press.
(34) J. J. Turner and M. Poliakoff, *J. Chem. Soc., Dalton Trans.*, 1351 (1973); J. J. Turner, private communication, and *J. Am. Chem. Soc.*, in press.
(35) M. Poliakoff, *J. Chem. Soc., Dalton Trans.*, 210 (1974).
(36) A. J. Rest, unpublished data cited in ref 35.
(37) H. Huber, E. P. Kündig, M. Moskovits, and G. A. Ozin, *J. Am. Chem. Soc.*, **97**, 2097 (1975).
(38) J. K. Burdett, *J. Chem. Soc., Chem. Commun.*, 763 (1973).
(39) D. McIntosh and G. A. Ozin, *J. Am. Chem. Soc.*, submitted for publication.
(40) S. F. A. Kettle, *J. Chem. Soc. A*, 420 (1966).